ISSN 1948-0210 (online)

World Journal of *Stem Cells*

World J Stem Cells 2019 February 26; 11(2): 55-146

Published by Baishideng Publishing Group Inc

WJSC

World Journal of Stem Cells

Contents

Monthly Volume 11 Number 2 February 26, 2019

Contents

World Journal of Stem Cells

Volume 11 Number 2 February 26, 2019

ABOUT COVER

Associate Editor of *World Journal of Stem Cells*, Dong-Wook Han, PhD, Professor, Department of Optics and Mechatronics Engineering, Pusan National University, Busan 46241, South Korea

AIMS AND SCOPE

World Journal of Stem Cells (*World J Stem Cells*, *WJSC*, online ISSN 1948-0210, DOI: 10.4252), is a peer-reviewed open access academic journal that aims to guide clinical practice and improve diagnostic and therapeutic skills of clinicians.

WJSC covers topics concerning all aspects of stem cells: embryonic, neural, hematopoietic, mesenchymal, tissue-specific, and cancer stem cells; the stem cell niche, stem cell genomics and proteomics, *etc*.

We encourage authors to submit their manuscripts to *WJSC*. We will give priority to manuscripts that are supported by major national and international foundations and those that are of great basic and clinical significance.

INDEXING/ABSTRACTING

The *WJSC* is now indexed in PubMed, PubMed Central, Science Citation Index Expanded (also known as SciSearch®), Journal Citation Reports/Science Edition, Biological Abstracts, and BIOSIS Previews. The 2018 Edition of Journal Citation Reports cites the 2017 impact factor for *WJSC* as 4.376 (5-year impact factor: N/A), ranking *WJSC* as 7 among 24 journals in Cell and Tissue Engineering (quartile in category Q2), and 65 among 190 journals in Cell Biology (quartile in category Q2).

RESPONSIBLE EDITORS FOR THIS ISSUE

Responsible Electronic Editor: *Ying-Na Bian* **Proofing Editorial Office Director:** *Jin-Lei Wang*

NAME OF JOURNAL
World Journal of Stem Cells

ISSN
ISSN 1948-0210 (online)

LAUNCH DATE
December 31, 2009

FREQUENCY
Monthly

EDITORS-IN-CHIEF
Tong Cao, Shengwen Calvin Li, Carlo Ventura

EDITORIAL BOARD MEMBERS
https://www.wjgnet.com/1948-0210/editorialboard.htm

EDITORIAL OFFICE
Jin-Lei Wang, Director

PUBLICATION DATE
February 26, 2019

INSTRUCTIONS TO AUTHORS
https://www.wjgnet.com/bpg/gerinfo/204

GUIDELINES FOR ETHICS DOCUMENTS
https://www.wjgnet.com/bpg/GerInfo/287

GUIDELINES FOR NON-NATIVE SPEAKERS OF ENGLISH
https://www.wjgnet.com/bpg/gerinfo/240

PUBLICATION MISCONDUCT
https://www.wjgnet.com/bpg/gerinfo/208

ARTICLE PROCESSING CHARGE
https://www.wjgnet.com/bpg/gerinfo/242

STEPS FOR SUBMITTING MANUSCRIPTS
https://www.wjgnet.com/bpg/GerInfo/239

ONLINE SUBMISSION
https://www.f6publishing.com

World Journal of Stem Cells

Submit a Manuscript: https://www.f6publishing.com

World J Stem Cells 2019 February 26; 11(2): 100-123

DOI: 10.4252/wjsc.v11.i2.100

ISSN 1948-0210 (online)

ORIGINAL ARTICLE

Basic Study

Triple-modal imaging of stem-cells labeled with multimodal nanoparticles, applied in a stroke model

Helio Rodrigues da Silva, Javier Bustamante Mamani, Mariana Penteado Nucci, Leopoldo Penteado Nucci, Andrea Tiemi Kondo, Daianne Maciely Carvalho Fantacini, Lucas Eduardo Botelho de Souza, Virginia Picanço-Castro, Dimas Tadeu Covas, José Mauro Kutner, Fernando Anselmo de Oliveira, Nelson Hamerschlak, Lionel Fernel Gamarra

ORCID number: Helio Rodrigues da Silva (0000-0002-1173-745X); Javier Bustamante Mamani (0000-0001-5038-0070); Mariana Penteado Nucci (0000-0002-1502-9215); Leopoldo Penteado Nucci (0000-0002-1234-5845); Andrea Tiemi Kondo (0000-0002-4228-8503); Daianne Maciely Carvalho Fantacini (0000-0003-2694-0132); Lucas Eduardo Botelho de Souza (0000-0003-4254-7509); Virginia Picanço-Castro (0000-0002-3914-0938); Dimas Tadeu Maciely Covas (0000-0002-7364-2595); José Mauro Kutner (0000-0003-3784-6731); Fernando Anselmo de Oliveira (0000-0002-7226-1694); Nelson Hamerschlak (0000-0002-5140-5310); Lionel Fernel Gamarra (0000-0002-3910-0047).

Author contributions: da Silva HR and Gamarra LF conceptualized the original idea; da Silva HR, Mamani JB, Nucci MP and Gamarra LF designed and performed the experiments and analyzed the data; Nucci LP and de Oliveira FA performed analysis of the data and animal management; Fantacini DMC, de Souza LEB, Picanço-Castro V and Covas DT performed the cellular culture for transduction of luciferase and the writing of the original draft; Kondo AT, Kutner JM, Nucci LP and Hamerschlak N performed the stem cell isolation and immunophenotype characterization; Mamani JB, Nucci

Helio Rodrigues da Silva, Javier Bustamante Mamani, Andrea Tiemi Kondo, José Mauro Kutner, Fernando Anselmo de Oliveira, Nelson Hamerschlak, Lionel Fernel Gamarra, Hospital Israelita Albert Einstein, São Paulo 05651-900, Brazil

Mariana Penteado Nucci, LIM44, Hospital das Clinicas HCFMUSP, Faculdade de Medicina, Universidade de São Paulo, São Paulo 05403-010, Brazil

Leopoldo Penteado Nucci, Centro Universitário do Planalto Central, Brasilia 72445-020, Brazil

Daianne Maciely Carvalho Fantacini, Lucas Eduardo Botelho de Souza, Virginia Picanço-Castro, Dimas Tadeu Covas, Faculdade de Medicina de Ribeirão Preto, Universidade de São Paulo, São Paulo 05403-010, Brazil

Corresponding author: Lionel Fernel Gamarra, PhD, Senior Scientist, Group of nanobiotechnology of The Albert Einstein Hospital, Hospital Israelita Albert Einstein, Avenida Albert Einstein, 627/701 - Morumbi, São Paulo 05651-900, Brazil. lgamarra@einstein.br
Telephone: +55-11-21510243

Abstract

BACKGROUND

Mesenchymal stem cells (MSCs) have been widely tested for their therapeutic efficacy in the ischemic brain and have been shown to provide several benefits. A major obstacle to the clinical translation of these therapies has been the inability to noninvasively monitor the best route, cell doses, and collateral effects while ensuring the survival and effective biological functioning of the transplanted stem cells. Technological advances in multimodal imaging have allowed *in vivo* monitoring of the biodistribution and viability of transplanted stem cells due to a combination of imaging technologies associated with multimodal nanoparticles (MNPs) using new labels and covers to achieve low toxicity and longtime residence in cells.

AIM

To evaluate the sensitivity of triple-modal imaging of stem cells labeled with MNPs and applied in a stroke model.

METHODS

After the isolation and immunophenotypic characterization of human bone

MP, Nucci LP and Gamarra LF did the writing - original draft and writing - review and editing; Gamarra LF performed funding acquisition, investigation, project administration, resources and supervision.

Supported by Conselho Nacional de Desenvolvimento Científico e Tecnológico, No. CNPq-465259/2014-6, and No. CNPq-400856/2016-6; São Paulo State Research Support Foundation, No. 2014/50983-3, and No. 2016/21470-3.

Institutional review board statement: The study was approved by the Ethics Committee for Research at the Instituto Israelita de Ensino e Pesquisa Albert Eisntein, Brazil (CAAE - 27665714.4.0000.0071) for the use of human mesenchymal stem cells after the donors informed consent.

Institutional animal care and use committee statement: The study was approved by the Ethics in Animal Research Committee of the Hospital Israelita Albert Einstein (HIAE) with approval number 1906-13. The vivarium of the Experimental Surgical Training Center (Centro de Experimentação e Treinamento em Cirurgia - CETEC) was accredited by the Association for the Assessment and Accreditation of Laboratory Animal Care International (AAALAC International).

Conflict-of-interest statement: The authors have declared that no competing interests exist.

Data sharing statement: The datasets supporting the conclusions of this article are included within in the article.

ARRIVE guidelines statement: The authors have read the ARRIVE guidelines - Animal Research: Reporting *In vivo* Experiments, and the manuscript was prepared and revised according to the ARRIVE guidelines.

marrow MSCs (hBM-MSCs), our team carried out lentiviral transduction of these cells for the evaluation of bioluminescent images (BLIs) *in vitro* and *in vivo*. In addition, MNPs that were previously characterized (regarding hydrodynamic size, zeta potential, and optical properties), and were used to label these cells, analyze cell viability *via* the 3-[4,5-dimethylthiazol-2-yl]-2,5 diphenyl tetrazolium bromide assay and BLI analysis, and quantify the internalization process and iron load in different concentrations of MNPs *via* magnetic resonance imaging (MRI), near-infrared fluorescence (NIRF), and inductively coupled plasma-mass spectrometry (ICP-MS). In *in vivo* analyses, the same labeled cells were implanted in a sham group and a stroke group at different times and under different MNP concentrations (after 4 h or 6 d of cell implantation) to evaluate the sensitivity of triple-modal images.

RESULTS

hBM-MSC collection and isolation after immunophenotypic characterization were demonstrated to be adequate in hBM samples. After transduction of these cells with luciferase (hBM-MSC$_{Luc}$), we detected a maximum BLI intensity of 2.0 x 10^8 photons/s in samples of 10^6 hBM-MSCs. Analysis of the physicochemical characteristics of the MNPs showed an average hydrodynamic diameter of 38.2 ± 0.5 nm, zeta potential of 29.2 ± 1.9 mV and adequate colloidal stability without agglomeration over 18 h. The signal of iron load internalization in hBM-MSC$_{Luc}$ showed a close relationship with the corresponding MNP-labeling concentrations based on MRI, ICP-MS and NIRF. Under the highest MNP concentration, cellular viability showed a reduction of less than 10% compared to the control. Correlation analysis of the MNP load internalized into hBM-MSC$_{Luc}$ determined *via* the MRI, ICP-MS and NIRF techniques showed the same correlation coefficient of 0.99. Evaluation of the BLI, NIRF, and MRI signals *in vivo* and *ex vivo* after labeled hBM-MSC$_{Luc}$ were implanted into animals showed differences between different MNP concentrations and signals associated with different techniques (MRI and NIRF; 5 and 20 μg Fe/mL; $P < 0.05$) in the sham groups at 4 h as well as a time effect (4 h and 6 d; $P < 0.001$) and differences between the sham and stroke groups in all images signals ($P < 0.001$).

CONCLUSION

This study highlighted the importance of quantifying MNPs internalized into cells and the efficacy of signal detection under the triple-image modality in a stroke model.

Key words: Multimodal nanoparticles; Human bone marrow mesenchymal stem cells; Near-infrared fluorescence image; Magnetic resonance image; Bioluminescence; Stroke

Core tip: Multimodal imaging techniques provide morpho-functional information for studying pathological events following ischemia associated with new tracers. Molecular imaging innovations will contribute to the further understanding of stem cell transplantation, allowing an assessment of their therapeutic effects at the molecular scale. In this study, we evaluate the sensitivity of triple-modal imaging of human bone marrow mesenchymal stem cells labeled with multimodal nanoparticles (MNPs) to quantify the internalized iron load and cellular viability as well as the correlation of quantification results between the techniques. We demonstrate the importance of quantifying the MNP load internalized into cells *via* triple-image evaluation and the efficacy of signal detection in a stroke model.

Citation: da Silva HR, Mamani JB, Nucci MP, Nucci LP, Kondo AT, Fantacini DMC, de Souza LEB, Picanço-Castro V, Covas DT, Kutner JM, de Oliveira FA, Hamerschlak N, Gamarra LF. Triple-modal imaging of stem-cells labeled with multimodal nanoparticles, applied in a stroke model. *World J Stem Cells* 2019; 11(2): 100-123
URL: https://www.wjgnet.com/1948-0210/full/v11/i2/100.htm
DOI: https://dx.doi.org/10.4252/wjsc.v11.i2.100

Manuscript source: Unsolicited manuscript

Received: October 22, 2018
Peer-review started: October 23, 2018
First decision: November 14, 2018
Revised: December 5, 2018
Accepted: December 17, 2018
Article in press: December 17, 2018
Published online: February 26, 2019

INTRODUCTION

Mesenchymal stem cells (MSCs) have been widely tested for therapeutic efficacy in the ischemic brain. The important roles of paracrine and immune modulatory mechanisms in the beneficial effects exerted by MSCs have been recognized in many studies[1]. Due to the relative ease of isolation, low immunogenicity, and good proliferation, differentiation, and paracrine potential of MSCs, these stem cells have become the main source for tissue engineering of bone, cartilage, muscle, marrow stroma, fat, and other connective tissues[2]. Moreover, we and others have shown that cellular therapy using MSC transplantation has the potential to improve the symptoms of various aging diseases, such as Parkinson's disease, stroke, amyotrophic lateral sclerosis, and multiple sclerosis[1,2].

Several preclinical investigations have indicated that the MSCs are unable to replace dead neurons following ischemic events; nevertheless, they provide various other types of benefits *via* parallel processes, including growth factor upregulation at the injured site, decreasing apoptosis, reducing glial scar formation, promoting axonal outgrowth, synaptic remodeling, neurogenesis, angiogenesis, and astrocyte and oligodendrocyte growth factors[1]. Intravenous injection is an often-used route for the delivery of MSCs in pre-clinical and clinical trials[3]. It was recently discovered that a large proportion of MSCs injected intravenously are trapped in the pulmonary vasculature, leading to a low delivery efficiency to target organs[4]. Nevertheless, it remains difficult to non-invasively monitor the delivery and biodistribution of administered cells in target organs in a quantitative way over a long period, without relying on behavioral endpoints or tissue histology[5].

Therefore, a major obstacle to the clinical translation of these therapies has been the inability to noninvasively monitor the best route, cell doses, and collateral or epigenomic effects, while ensuring survival and the effective biological functioning of the transplanted stem cells[6].

Consequently, there is a need for technological advances in the development of non-invasive imaging techniques with a high spatial and temporal resolution that allow *in vivo* monitoring of the biodistribution and viability of transplanted stem cells[7]. These requirements can be met through a combination of imaging technologies, also known as multimodal imaging[8]. In parallel with this increase in technological image-based verification, multimodal nanoparticles (MNPs) have been developed to show lower toxicity and an increased residence time in cells with the use of new labels and covers[9].

Currently, multimodal imaging techniques provide morpho-functional information at different times, which improves the field of diagnostic imaging, in addition to generating detailed information on diseases from multiple images and allowing simultaneous diagnosis and therapy[10]. Technological innovations and the development of new tracers and smart probes have further promoted these multimodal imaging techniques, providing safe improvement of contrast and multidimensional functional, structural and morphological information[9].

Superparamagnetic iron oxide nanoparticles (SPIONs), which are known for their magnetic properties (superparamagnetic), biocompatibility, biodegradability, surface-to-volume ratio, and greater surface area (sizes as small as 100 nm), exhibit diverse potential applications, such as drug delivery for magnetic resonance imaging (MRI), diagnostics, specific cell labeling and tracking of cell separation and bio-catalysis. Surface modification with polymeric stabilizers and inorganic molecules (*e.g.*, silica, gold, gadolinium, fluorescent dyes) increases sensibility and specificity in certain medical diagnoses, thus making this approach ideal for increasing accuracy in many biomedical applications[11].

SPION labeling with near-infrared (NIR) dye, which further improves probe capabilities, reveals deeper tissue penetration due to minimal absorbency of the surface tissue in the spectral region[12]. *In vivo* fluorescence imaging has undergone remarkable growth with the use of the novel NIR fluorescence (NIRF) probes and optical instruments that allow evaluation of the dynamic migration and distribution of transplanted MSCs as well as the stem cell-based regeneration of tissue[13].

The bioluminescent imaging (BLI) technique is complementary to NIRF imaging, enhancing the monitoring of ischemic and inflammation processes and viable cells after engraftment reduction. The BLI method requires genetic modification of cells to express the luciferase enzyme signal. Despite the low spatial resolution, the resulting images exhibit a good temporal resolution, and cell morphology is not altered[14].

Promising studies have focused on engineering MSCs for targeted delivery in specific targets. Additional efforts would benefit from imaging technologies for quantitatively monitoring *in vivo* cell localization and in real time[15]. One previous study by our group examining *in vivo* dual-modal imaging techniques (MRI combined with NIRF) and cytology demonstrated that the infused labeled cells could be

efficiently tracked in a Parkinson`s disease model. However, cellular viability could not be assessed due to the lack of another imaging modality[16]. Therefore, the present study aimed to evaluate two procedures: (1) we evaluate the sensitivity of triple-modal imaging (NIRF, MRI and BLI) of stem cells labeled with multimodal nanoparticles for quantification of the iron load internalized and cellular viability *in vitro* as well as the correlation of quantification results between the techniques of inductively coupled plasma-mass spectrometry (ICP-MS), MRI and NIRF; (2) we verify whether the images of stem cells labeled with multimodal nanoparticles maintain the same properties after application in a stroke model.

MATERIALS AND METHODS

In vitro study

Isolation and culture of human bone marrow MSCs: hMSCs were isolated from the bone marrow of normal donors who had provided informed consent for the research project (CAAE - 27665714.4.0000.0071), which was approved by the ethics committee for research at the Instituto Israelita de Ensino e Pesquisa Albert Eisntein (São Paulo, Brazil).

The aspirated bone marrow was diluted with phosphate-buffered saline (PBS) (Gibco®, Carlsbad, CA, United States) (1:3) then centrifuged with 20 mL of Ficoll/Hypaque (GE Healthcare) for 30 min at 500 *x*g and 22 °C. Following centrifugation, the cells were removed from the plasma/Ficoll-Hypaque interface, washed 3 times with PBS, and resuspended in Dulbecco's modified Eagle's medium - high glucose (DMEM-HG) (Gibco®, Carlsbad, CA, United States) supplemented with 15% fetal bovine serum (FBS) (Gibco®, Carlsbad, CA, United States).

The hBM-MSCs were cultivated in 75 cm^2 flasks with DMEM - low glucose (DMEM-LG) (GIBCO - Invitrogen Technologies, New York, USA), supplemented with 10% FBS, 1% de L-glutamine, 100 U/mL streptomycin and 100 U/mL penicillin (GIBCO - Invitrogen Technologies, New York, United States) and were maintained in humidified incubators with 5% CO_2 at 37 ºC, to favor the attachment of cells to the flask bottom.

Immunophenotypic characterization of hBM-MSCs: Cell-surface expression was analyzed with a predefined set of protein markers. In brief, cells at the third passage with 70% confluency were stained with the selected monoclonal antibodies and incubated in the dark for 30 min at 4 ºC. The cells were then washed and fixed with 1% paraformaldehyde. The following positive human marker antibodies were used: CD29-PE (clone: MAR4; BD Pharmingen), CD44-PE (clone: 515; BD Pharmingen), CD73-PE (clone: AD2; BD Pharmingen), CD90-APC (clone: 5E10; BD Pharmingen), and CD105-PE (clone: 8E11; Chemicon, Temecula, CA, United States). The negative markers were as follows: CD14-FITC (clone: M5E2; BD Pharmingen, San Diego, CA, United States), CD19-APC (clone: SJ25C1; Biosciences), CD31-PE (clone: WM59; BD Pharmingen), CD34-PE (clone: 581; BD Pharmingen), CD45-PerCP-Cy5 (clone: 2D1; Biosciences, San Jose, CA, United States), CD106-FITC (clone: 51-10C9; BD Pharmingen), and human leukocyte antigen HLA-DR-PerCPCy5 (clone: L243; Biosciences). The cells were analyzed using FACSARia flow cytometry equipment (Becton Dickinson, San Jose, CA, United States), and the acquired data were analyzed using FLOWJO (Tree Star, Ashland, OR) software.

The hBM-MSCs were also subjected to differentiation induction to evaluate the multipotentiality characteristics and differentiation capacity of the cells into two cellular types: adipocytes and osteoblasts.

Lentiviral transduction of hBM-MSCs for BLI analysis: Cells were genetically engineered to generate luciferase-expressing hBM-MSCs (hBM-MSC_{Luc}). Briefly, hBM-MSCs were transduced with the glycoprotein of the vesicular stomatitis virus (VSV-G) from pseudotyped viruses carrying the lentiviral vector (pMSCV_Luc2_T2A_Puro). The vector encodes the bioluminescent reporter luciferase-2 and the puromycin resistance gene puromycin N-acetyl-transferase under the control of a murine stem cell virus (MSCV) promoter.

For virion production, human embryonic kidney 293FT cells grown at 80% confluence in 150 mm Petri dishes (about 20 million cells/dish) were simultaneously transfected with 30 μg/dish of the vector pMSCV-Luc2-T2A-Puro along with two other helper vectors: 20 μg/dish of pCMV-dr8.91 and 10 μg/dish of pMD2.G. Transfection was conducted with 25-kDa linear polyethylenimine (PEI, Alfa Ansar) as previously reported[17]. Two days after transfection, the viral supernatant was collected and filtered through 0.45 μm polyvinylidene fluoride (PVDF) filters and concentrated by ultracentrifugation. As described in previous reports, the copy

number of integrated lentiviral vector sequences was determined *via* quantitative real-time polymerase chain reaction (PCR).

For lentiviral transduction, virions were added to cultures of 1 × 10^6 hBM-MSCs at a multiplicity of infection of 3 (MOI = 3) in the presence of 8 μg/mL polybrene (Sigma-Aldrich). The medium was replaced after 18 h, and the cells were cultured for an additional 48 h. After this period, the cells were selected for incubation with 1 μg/mL puromycin every other day for 8 d.

Bioluminescence signal expression in hBM-MSC$_{Luc}$: The expression of the bioluminescence (BLI) signal in hBM-MSC$_{Luc}$ was analyzed in the following cell concentrations/well: 1 × 10^4, 1 × 10^5 and 1 × 10^6, in triplicate samples in a 24-well plate, using IVIS® Lumina LT Series III equipment (Xenogen Corp. CA, EUA). Images were captured before and after the addition of 100 μL of D-luciferin (50 mg/mL) (XenoLight, PerkinElmer), and the intensity of the BLI signal was detected under the following parameters: Exposure time of 2 ms with a 5 min interval between each image acquisition, over a total of 490 min. The kinetics of BLI expression were registered and analyzed with Living Image Software version 4.3.1 (IVIS Imaging System) in radiation absolute units (photons/s).

MNP with magnetic and fluorescent properties: We used multimodal nanoparticles (MNP-IR750; Molday ION™750 - BioPal) with an 8 nm iron oxide (Fe_3O_4) nucleus, a hydrodynamic size of 35 nm (coated with dextran), and a zeta potential of approximately +31 mV, which were conjugated with fluorophores that emitted fluorescence with of NIR absorption/emission wavelengths of 755/777 nm. The MNP-IR750 has magnetic and fluorescent properties detectable in MRI and NIR images.

MNP-IR750 characterization: Hydrodynamic size, zeta potential and optical properties: The hydrodynamic size and zeta potential of MNP-IR750 were measured using the dynamic light scattering (DLS) technique with the Zetasizer Nano S system (Malvern, United Kingdom). The hydrodynamic size distribution was obtained at an angle of 173°, with the number of averages set at 20 and a time of 5 s per mean. Measurements were performed in a fixed position at 25 °C with a 60 s equilibrium period. In addition, to obtain information about possible agglomeration of nanoparticles, we performed an analysis of the stability of MNP-IR750 using DMEM-LG supplemented with 10% FBS over 18 h. The hydrodynamic size and zeta potential (surface charge) measurements were performed at a concentration of 50 μg Fe/mL and a pH of 7.4.

To verify the optical properties of MNP-IR750 excitation/emission, the corresponding spectrum was acquired using a Shimadzu RF-6000 fluorometer at a concentration of 100 μg Fe/mL, maintaining the temperature at 37 °C.

hBM-MSC$_{Luc}$ labeled with MNP-IR750: For hBM-MSC$_{Luc}$ labeling with MNP-IR750, triplicate samples of 1 × 10^4 cells were placed in a 24-well plate in DMEM-LG, supplemented with 15% FBS, penicillin (100 U/mL), streptomycin (100 μg/mL) and 1% L-glutamine. After 24 h of hBM-MSC$_{Luc}$ adhesion, the cells were washed twice with 300 μL of PBS and incubated for 18 h (at 37 °C and 5% CO_2), with MNP-IR750 added at the following concentrations: 5, 10, 20, 30, 40 and 50 μg Fe/mL, in DMEM-LG supplemented with 15% FBS. After incubation, the culture medium was removed, and the cells were washed three times with PBS.

Following the labeling of hBM-MSC$_{Luc}$ with MNP-IR750, the evaluation of MNP-IR750 internalized was performed *via* MRI, NIRF and BLI, and the viability of the labeled cells was assessed *via* the 3-[4,5-dimethylthiazol-2-yl]-2,5 diphenyl tetrazolium bromide (MTT) assay and the BLI technique.

Internalization of MNP-IR750 into hBM-MSC$_{Luc}$: Confirmation of the labeling of hBM-MSC$_{Luc}$ with MPN-IR750 was performed at the following concentrations: 5, 10, 20, 30, 40 and 50 μg/mL of MNP-IR750 in culture plates, *via* Prussian Blue staining[16,18]. Cells that were previously labeled and fixed in plates were washed twice with PBS and incubated with a staining solution composed of 0.25 mg of potassium ferrocyanide [K4Fe(CN)$_6$] (SIGMA, United States) and 5% hydrochloric acid (HCl) in a proportion of 1:1, in a volume of 1000 μL per well over 5 min at room temperature, protected from light. After this period, the Prussian Blue solution was removed, and the wells containing hBM-MSC$_{Luc}$ were washed twice with 500 μL of PBS. Thereafter, 500 μl of Nuclear Fast Red staining solution (SIGMA, United States) was added to the wells, followed by incubation for 10 min. After staining, the cells were washed again with PBS (2x), and light-field images were obtained under a Nikon TI® inverted microscope.

MRI, NIRF and BLI signals after internalization of MNP-IR750 by hBM-MSC$_{Luc}$: MRI, NIRF and BLI signals were evaluated in hBM-MSC$_{Luc}$ after labeling with MNP-IR750 at the following concentrations: 5, 10, 20, 30, 40 and 50 μg/mL.

For MRI signal evaluation, the labeled hBM-MSC$_{Luc}$ were mixed with 1% agarose (Sigma-Aldrich Chemie GmbH, Germany) and plated in culture wells. Images were acquired on a 3T RM scanner with a head coil of 32 channels (Magnetom Vision, Siemens, Germany) using the T2-weighted imaging sequence, following the protocol described in a previous study[19].

NIRF and BLI images were acquired after the plating of labeled hBM-MSC$_{Luc}$. The BLI signal was acquired after the addition of 100 μL of luciferin (1 mmol/L in PBS), the maximum time of intensity of the BLI signal determined *via* kinetic BLI analysis (section 2.4), using an exposure time of 2 ms, binning of 2 and f/stop of 4. The NIRF signal was acquired in the same samples used for BLI, applying an excitation of 745 nm, registered in a range of emission of 810-875 nm. Both imaging analyses were performed with IVIS® Lumina LT Series III equipment, and the signals were analyzed in radiation absolute units (photons/s). The experiments were performed with hBM-MSC$_{Luc}$ between the fifth and seventh passages.

Viability of hBM-MSC$_{Luc}$ labeled with MNP-IR750 - MTT and BLI: Evaluation of the viability of hBM-MSC$_{Luc}$ labeled with MNP-IR750 was performed using the MTT and BLI assays.

In the MTT assay, hBM-MSC$_{Luc}$ were grown in 96-well plates until they were subconfluent. MPN-IR750 were then added to the cells at defined concentrations of 5, 10, 20, 30, 40 and 50 μg Fe/mL, followed by incubation overnight. After incubation, the culture medium was discarded, and 100 μL of fresh medium per well was added to the cells, after thorough washing with PBS. Then, 100 μL of the MTT reagent (1 mg/mL - final concentration) was added per well, and the plate was incubated for four h in an incubator, at 37 °C in 5% CO_2. Actinomycin D (Sigma-Aldrich) was used as positive control for cell death in this assay. The "cell death dose" concentration identified in this assay was 0.25 μg/mL. After incubation, the medium was discarded from the wells, and 100 μL of dimethyl sulphoxide (DMSO Hybri-Max - Sigma-Aldrich) was added to solubilize the formazan crystals that had formed. Readings were then taken in a DTX 880 Multimode Detector reader (Beckman Coulter) at 490 nm, with subtraction for plate absorbance at 650 nm. The viability percentage of the cells was calculated as the ratio of the mean absorbance of triplicate readings with respect to the mean absorbance of control wells, as cell viability = (sample/control) × 100.

The viability assays were verified using the BLI technique. Similar samples to those used in the MTT assays were used for the BLI assay, adding 100 mL of luciferin in each well, and acquiring the BLI images using IVIS® Lumina LT Series III equipment. For BLI intensity analysis (photons/s), a region of interest (ROI) of 2.5 cm^2 was selected. The viability percentage was calculated with the formula (sample/control) × 100.

Quantification of MNP-IR750 internalized into hBM-MSC$_{Luc}$: Quantification of MNP-IR750 after hBM-MSC$_{Luc}$ labeling was performed *via* MRI, ICP-MS and NIR imaging. The samples used for quantification were prepared with 1 × 10^6 hBM-MSC$_{Luc}$ that either were not labeled (control) or were labeled with MNP-IR750 at the following concentrations: 5, 10, 20, 30, 40 and 50 μg Fe/mL.

Quantification of MNP-IR750 internalized into hBM-MSC$_{Luc}$*via* MRI. For quantification of the internalization process by MRI, the following equation was used:

(1) $1/(T_2^{\text{hBM-MSC}_{Luc}+\text{MNP\_IR750}}) = 1/(T_2^{\text{hBM-MSC}_{Luc}}) + [Fe] \times r_2$

where [Fe] is the concentration of intracellular iron internalized into hBM-MSC$_{Luc}$; r_2 is the relaxivity of the MNP-IR750; and T_2 is the transverse relaxation time for samples containing hBM-MSC$_{Luc}$ labeled with MNP-IR750 and control samples (hBM-MSC$_{Luc}$).

For the calculation of r_2, a phantom with 24 wells (culture plate) containing MNP-IR750 suspended in the following concentrations was used: 0, 2, 4, 6, 10, 15 and 20 μg Fe/mL, dispersed in 1% agarose. The phantom was subjected to MRI examination and the T_2 values of samples were determined from the relaxivity curves. The r_2 values were obtained *via* linear adjustment of the inverse of the transverse relaxation *vs* the concentration of MNP-IR750 used for cellular labeling.

For the calculation of $T_2^{\text{hBM-MSC}_{Luc}+\text{MNP\_IR750}}$, samples labeled with different concentrations of nanoparticles, as described above, were used; for the determination of $T_2^{\text{hBM-MSC}_{Luc}}$, only 1 × 10^6 hBM-MSC$_{Luc}$ from the samples were used. In both analyses, the samples were suspended in a 1% agarose solution and plated in a 24-well culture plate, then subjected to MRI examination.

T_2-weighted MRI images were acquired in a whole-body 3T scanner (Magneton Vision®, Siemens, Erlangen, Germany) with a 32-channel head coil using the following

parameters: Multicontrast turbo-spin echo sequence, repetition time (TR) of 1500 ms, echo time (TE) of 8-256 ms, field of view of 300 mm, 256 × 256 matrix, slice thickness of 3.0 mm and flip angle of 180°. The intensity curves of the MRI signals of the samples as a function of TE were analyzed using a selection of regions of interest with a fixed size. The T_2 of each sample was determined by adjusting the decay curve with a monoexponential linear algorithm: Intensity (TE) = C × $e^{(-TE/T2)}$.

From the MNP-IR750 load obtained from equation 1, the number of MNP-IR750 internalized into hBM-MSC_{Luc} was calculated with the following equation:

(2) Number of MNP_IR750 = $[6 \times load_{MNP\_IR750} \times (at\_m)]/[\pi \times \rho_{MNP\_IR750} \times M_{Fe} \times \varphi^3_{MNP\_IR750}]$

Where $load_{MNP\_IR750}$ is the internalization MNP-IR750 loaded into hBM-MSC_{Luc}; at_m is the atomic mass; ρ_{MNP_IR750} is the iron oxide density (Fe_3O_4); M_{Fe} is the molecular weight of iron; and φ_{MNP_IR750} is the diameter of MNP-IR750.

Quantification of MNP-IR750 internalized into hBM-MSC_{Luc}*via* ICP-MS. The samples were diluted in 1 mL of Milli-Q® water (EMD Millipore Corporation, Bedford MA, USA) and subjected to the digestion of organic components with 5 mL of nitric acid (37%) using a Titan Microwave sample preparation system (Perkin Elmer, USA). After digestion, the samples were analyzed with ICP-MS equipment (Perkin Elmer Nexion 350x, PerkinElmer Corporation, USA) to determine the iron content of each sample. Measurements of samples were performed in triplicate, and quantification was based on a calibration curve using certified standard iron (NexION # N8145054) at the following concentrations: 0, 10, 20, 30, 40 and 50 ng Fe/mL (ppb). Samples of 1 × 10^6 hBM-MSC_{Luc} without labeling were used as a control.

Quantification of MNP-IR750 internalized into hBM-MSC_{Luc}*via* NIRF imaging. NIRF images were acquired after trypsinization of the samples and washing with PBS. The NIRF signal was detected after excitation at 745 nm and was registered in the emission range of 810-875 nm using IVIS® Lumina LT Series III equipment. The absolute quantification was determined after establishing the calibration curve using known concentrations of 1, 2, 3, 4, 5 and 6 μg Fe/mL.

In vivo study

Animals and experimental design: We used 2-month-old male Wistar rats weighing 250-300 g. The animals were maintained at the vivarium of the Experimental Surgical Training Center (Centro de Experimentação e Treinamento em Cirurgia - CETEC) at 21 ± 2°C and 60% ± 5% relative humidity with full ventilation under a 12 h light/dark cycle (7 a.m. - 7 p.m.), and they had access to food and water *ad libitum*. This vivarium is accredited by the Association for the Assessment and Accreditation of Laboratory Animal Care International (AAALAC International), and the general conditions were monitored daily. The study was approved by the Ethics in Animal Research Committee of the Hospital Israelita Albert Einstein (HIAE) with approval number 1906-13

The experimental design of the *in vivo* study involved in two experiments:

Experiment 1 was conducted to analyze the sensitivity of the NIRF, BLI and MRI signals of the labeled hBM-MSC_{Luc} implanted at different concentrations in the animals in the sham group, after being subjected to a craniectomy procedure. These animals were divided into 4 groups (n = 7 rats/group): Group Sham_control (S_control) - implantation of 1 × 10^6 de hBM-MSC_{Luc}; Group Sham_5 - implantation of 1 × 10^6 de hBM-MSC_{Luc} labeled with 5 μg Fe/mL of MPN-IR750; Group Sham_20 implantation of 1 × 10^6 de hBM-MSC_{Luc} labeled with 20 μg Fe/mL of MPN-IR750; and Group Sham_50 implantation of 1 × 10^6 de hBM-MSC_{Luc} labeled with 50 μg Fe/mL of MPN-IR750.

Experiment 2 analyzed the NIRF, BLI and MRI signals of the labeled hBM-MSC_{Luc} implanted in the animals after being subjected to stroke induction. These animals were divided into 2 groups (n = 7 rats/group): Group Sham_50: implantation of 1 × 10^6 de hBM-MSC_{Luc} labeled with 50 μg Fe/mL of MPN-IR750; and Group Stroke_50: implantation of 1 × 10^6 de hBM-MSC_{Luc} labeled with MPN-IR750. The concentration of nanoparticles that was used was determined from the best conditions verified in experiment 1.

In both experiments, the animals were randomly allocated, coded and housed in individual cages.

Evaluation of NIRF, BLI and MRI signals after the implantation of hBM-MSC_{Luc} labeled with MNP-IR750 in animals (Experiment 1): A total of 28 Wistar rats were used to evaluate the behavior of the signals of the labeled and unlabeled hBM-MSC_{Luc} in the animals' brains. The animals were anesthetized with ketamine hydrochloride (100 mg/kg) and xylazine hydrochloride (20 mg/kg) i.p. and subjected to a craniectomy procedure to implant the cells at the following coordinates: 2.0 mm antero-posterior, 2.0 mm lateral to the midline and 2.5 mm deep, according to the

atlas of Paxinos and Watson (1986)[20]. The cells were infused at a rate of 10 μL/min using a 10 μL Hamilton syringe.

After 4 h of cell implantation, the animals were subjected to evaluation of BLI expression and NIRF detection *in vivo* using IVIS® Lumina LT Series III equipment. The NIRF signal measurements were obtained with an excitation wavelength of 745 nm and an emission wavelength of 810-875 nm. Soon thereafter, the animals received 150 mg/kg of luciferin i.p., and the BLI images were acquired with 10 min of latency. Both images were analyzed in radiation absolute units (photons/s).

The animals were euthanized after *in vivo* NIRF and BLI evaluation. Their brains were extracted to record NIRF emissions using the same parameters employed for *in vivo* image acquisition. Following *ex vivo* NIRF analysis, the brains were fixed with 4% paraformaldehyde, and brain phantoms were prepared with 1% agarose for MRI signal evaluation. The phantoms with brain tissue were analyzed by using a 3T scanner (Siemens), to track the hBM-MSC$_{Luc}$ labeled with MNP-IR750. The MRI images were obtained with a 3D Fast Low Angle Shot (FLASH) sequence, a matrix of 256x160x128, TR = 200 ms, TE = 20 ms, and a range of excitation angle of 20-25º.

Induction of a focal ischemic lesion *via* thermocoagulation (stroke): A focal brain ischemic lesion was induced *via* thermocoagulation in the pial blood vessels of the motor and somatosensory cortex as previously described[21]. Briefly, animals were anesthetized with ketamine hydrochloride (100 mg/kg, i.p.) and xylazine hydrochloride (20 mg/kg, i.p.) and placed in a stereotaxic apparatus (Harvard Apparatus, Holliston, United States). A craniectomy procedure was performed to expose the left somatosensory cortex (+ 2 to -6 mm in the anterior-posterior direction and +2 mm on the medial-lateral axis from the Bregma, according to the atlas of Paxinos and Watson)[20]. Superficial blood vessels were transdurally thermocoagulated by approximation of a hot probe to the dura matter (about 2 mm), maintaining a constant temperature of 400ºC for 30 min. The procedure was concluded with incision tissue suturing and the administration of a tramadol analgesic (5 mg/kg) (i.p.). Throughout anesthesia, the rats were placed on a heating pad to maintain the rectal temperature at 37.0 ± 0.5 ºC (PhysioSuite, kent Scientific Corporation, Torrington, CT, United States).

The ischemic lesion was confirmed through local blood perfusion analysis using a PeriCam Perfusion Speckle Imager (PSI) system (Perimed, Stockholm, Sweden) and TTC staining after 2 h of lesion induction, as described in a previous study[21]. The color changes of the targeted region, from light red to dark red, were also noted[22].

Implantation of hBM-MSC$_{Luc}$ labeled with MNP-IR750 and evaluation of the signal in the brains of animals after focal ischemic lesion induction (Experiment 2): In experiment 2, after 24 hs of focal brain ischemic induction, the animals were subjected to cell implantation in the same manner described above in section 2.13. Then, 6 d after stroke induction, we analyzed the signal behavior of the hBM-MSC$_{Luc}$ labeled with MNP-IR750 *via* BLI and NIRF imaging *in vivo* and MRI *ex vivo*, following the same procedures described in section 2.13. The concentration of MNP-IR750 implanted in the stroke group was determined from the best result for the signal detected in the presence of the different concentrations tested in experiment 1.

Statistical analysis

Data were presented as the mean and standard deviation in each analysis. For the *in vivo* study, the quantification of the effect of the MNP-IR750 concentration in the sham group was compared *via* the ANOVA test, following Bonferroni-corrected post hoc tests for each image technique (experiment 1). For temporal analysis in the sham groups (4 h *vs* 6 d, experiments 1 and 2, respectively) and group analysis for experiment 2 (sham *vs* stroke at 6 d), Student's *t*-test was applied, with previous verification of a normal distribution and homoscedasticity in the two groups. Finally, we compared the differences between NIRF and MRI *via* an independent samples *t*-test.

RESULTS

Characterization of hBM-MSCs

After the isolation and culture of hBM-MSCs, immunophenotypic characterization was performed using flow cytometry, which showed that showed positive surface markers for CD29 (93.7%), CD44 (94.9%), CD 73 (95.0%), CD90 (94.7%) and CD105 (93.2%) as depicted in Figure 1A-E, negative surface markers for CD14 (0.17%), CD19(0.87%), CD31(1.35%), CD34(1.47%), CD45 (0.83%) and CD106 (0.96%), as depicted in Figure 1F-K, with low levels of HLA-DR (2.82%, Figure 1L). These results

confirmed the immunophenotypic profile of the hBM-MSCs and demonstrated that the collection and isolation of these cells from human bone marrow samples were adequate.

hBM-MSC$_{Luc}$ bioluminescence signal

The hBM-MSC$_{Luc}$ bioluminescence signal was analyzed as a function of the number of cells over 490 min showing the intensity of the signal curves (Figure 2), in which we observed a peak of intensity at 10 min, followed by a decrease in the BLI signal intensity over time. These patterns were observed for all concentrations of cells tested, and the highest cell concentrations corresponded to the highest amplitude curves.

Images of circular ROIs represented the BLI intensity over time for each concentration of cells. The color variations of the ROIs were determined from the intensity of the BLI signal for each part of the curve, as represented by a color scale of intensity (Figure 2, blue to red scale). The BLI intensity of 10^6 hBM-MSC$_{Luc}$ samples revealed a maximum of 2.0×10^8 photons/s (Figure 2, peak of the blue curve) after luciferin addition, but the BLI intensity was almost null under the same concentration (10^6 hBM-MSC$_{Luc}$) without luciferin addition (inset in Figure 2, black curve). The peaks of BLI intensity for 10^4 hBM-MSC$_{Luc}$ and 10^5 hBM-MSC$_{Luc}$ were 0.3×10^7 and 0.25×10^8 photons/s, respectively (Figure 2, pink and red curves).

MNP-IR750 characterization

Figure 3 shows the curves of the hydrodynamic size distribution of MPN-IR750 acquired over 18 h. The curves for a polydispersed log-normal size distribution showed an average hydrodynamic diameter of 38.2 ± 0.5 nm. The curves obtained temporally showed a constant distribution of the hydrodynamic diameter in DMEM-LG culture supplemented with 10% PBS. MNP-IR750 did not agglomerate in the period of time analyzed, showing adequate stability during the analysis.

The MNP-IR750 surface charge determined from the zeta potential at pH 7.4 was $\xi = +29.2 \pm 1.9$ mV, as shown in Figure 3B, indicating a positive potential of MNP-IR750 that favors the electrostatic process with hBM-MSC$_{Luc}$.

The fluorescence optical properties of MNP-IR750 revealed peaks of intensity in the excitation/emission spectrum at 757.9 nm (excitation) and 779.4 nm (emission), as shown in Figure 3C. These values correspond to the infrared spectrum, which indicates high applicability in *in vivo* studies, due to low absorption of biologic molecules in this region of the spectrum.

Evaluation of the internalization of MNP-IR750 by hBM-MSC$_{Luc}$

After labeling hBM-MSC$_{Luc}$ with MNP-IR750 at concentrations of 5, 10, 20, 30, 40 and 50 μg Fe/mL, Prussian blue staining was performed. The optical microscopy images showed that the presence of MNP-IR750 was highlighted, due to the blue staining of iron oxide nuclei in the hBM-MSCLuc cytoplasm (Figure 4 A-N), demonstrating the efficacy of cellular labeling at all MNP-IR750 concentrations.

In addition to the adequate labeling intensity, the cellular morphology was preserved under all labeling conditions. However, the intensity of labeling was dependent on the MNP-IR750 concentration used. The cells labeled with 5 μg/mL of MNP-IR750 exhibited lower labeling in comparison to the other concentrations tested. The difference was discrete between 10 and 20 μg/mL of MNP-IR750 (Figure 4E-H) and between 30, 40 and 50 μg/mL of MNP-IR750 (Figure 4I-N). The contrast between the 5 and 10 μg/mL concentrations of MNP-IR750 (Figure 4C, D and 4E, F, respectively) and between 20 and 30 μg/mL of MNP-IR750 (Figure 4G, H and 4I, J, respectively) was more evident than those between the other concentrations.

Evaluation of hBM-MSC$_{Luc}$ labeled with MNP-IR750 based on fluorescent properties was not possible *via* the fluorescence microscopy technique, as the emission/absorption spectrum is within the NIR range.

Evaluation of the viability of hBM-MSC$_{Luc}$ labeled with MNP-IR750: MTT and BLI assays

The cellular viability analysis of hBM-MSC$_{Luc}$ labeled with different concentrations of MNP-IR750 indicated a discrete increase in toxicity due to increasing concentrations of MNP-IR750 compared to the control sample (hBM-MSC$_{Luc}$ unlabeled) (Figure 4O).

Under standard culture conditions, unlabeled hBM-MSC$_{Luc}$ (control) showed 100% relative cellular viability in both assays (Figure 4O). Cellular viability determined *via* the MTT assay decreased as the MNP-IR750 concentration rose, where the lowest MNP-IR750 concentration (5 μg Fe/mL) resulted in a viability of 98.9%, and while a viability of 90.5% was observed for the highest concentration of MNP-IR750 (50 μg Fe/mL). The difference between the highest concentration of MNP-IR750 (50 μg Fe/mL) and the control was 9.5%, with remarkable differences being found between 5 and 10 μg Fe/mL of MNP-IR750 (2.2%), 20 and 30 μg Fe/mL of MNP-IR750 (1.6%)

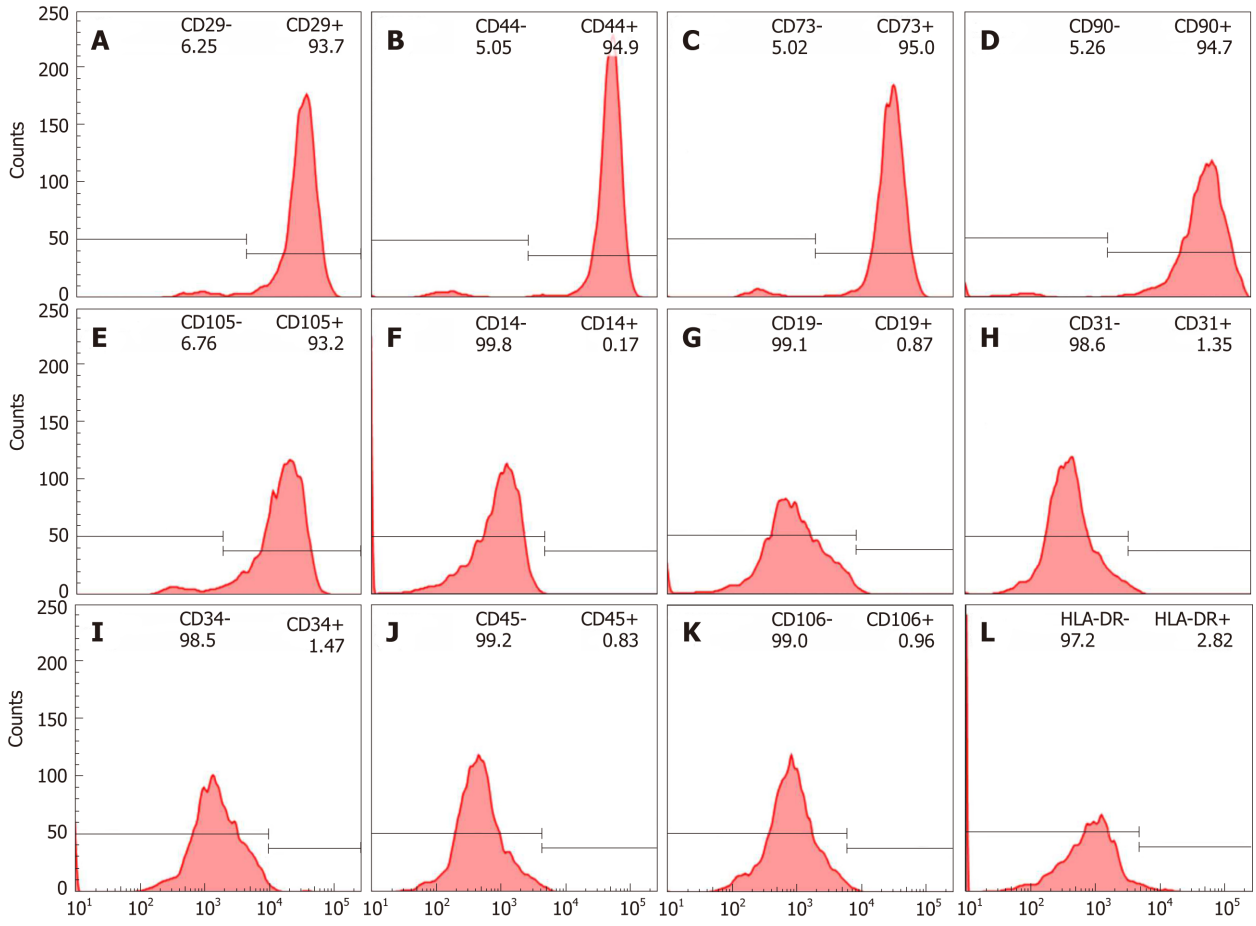

Figure 1 Immunophenotypic characterization of human bone marrow mesenchymal stem cells. A-D: Positive surface markers CD29, CD44, CD 73, CD90 and CD105; E-K: Negative surface markers CD14, CD19, CD31, CD34, CD45 and CD106; L: Low levels of HLA-DR.

and 30 and 40 μg Fe/mL of MNP-IR750 (3.0%). The lowest difference between the concentrations was found between 40 and 50 μg Fe/mL of MNP-IR750 (0.5%) (Figure 4O - red bars).

In the BLI assay, cellular viability decreased by 7.7% from the control to the highest concentration of MNP-IR750 (92.3% for 50 μg Fe/mL of MNP-IR750) (Figure 4O - blue bars). The viability observed under lower MNP-IR750 concentrations showed greater relevance (97.6% for 5 μg Fe/mL, 95.5% for 10 μg Fe/mL and 94.7% for 20 μg Fe/mL), while for the highest concentrations, viability was more constant (93.8% for 30 μg Fe/mL, 93.2% for 40 μg Fe/mL and 92.3% for 50 μg Fe/mL) (Figure 4O - blue bars).

The cellular viability showed dependence upon the dose applied but remained over 90% in both assays. Considering the small deviation observed for each MNP-IR750 concentrations, the viability values found in the MTT and BLI assays were highly similar.

Evaluation of MRI, NIRF and BLI signals after internalization of MNP-IR750 by hBM-MSC$_{Luc}$

After labeling hBM-MSC$_{Luc}$ with MNP-IR750 at concentrations of 5, 10, 20, 30, 40 and 50 μg Fe/mL, MRI images were acquired as a function of TE (Figure 5A, first and second phantom images). These images showed differences related to the different cellular concentrations and between short and long TEs (93.6 and 249.6 ms), mainly for the highest concentrations. From the MRI, it was possible to determine the T2 values presented in the gray columns of the graphic (Figure 5B), demonstrating that the signal decayed with the increase in the MPN-IR750 concentration for both TEs analyzed; a high signal intensity was also present when a short TE was used.

BLI and NIRF images were acquired with the same phantom used in MRI, but comparing the intensity signal before and after luciferin addition (Figure 5A, fourth and last phantom images). The NIRF images showed a discrete influence of the presence of luciferin during signal analysis (Figure 5C). However, considering the small discrepancy between the intensity values, the difference was actually practically null. The BLI intensity signal after luciferin addition showed a reduction with the

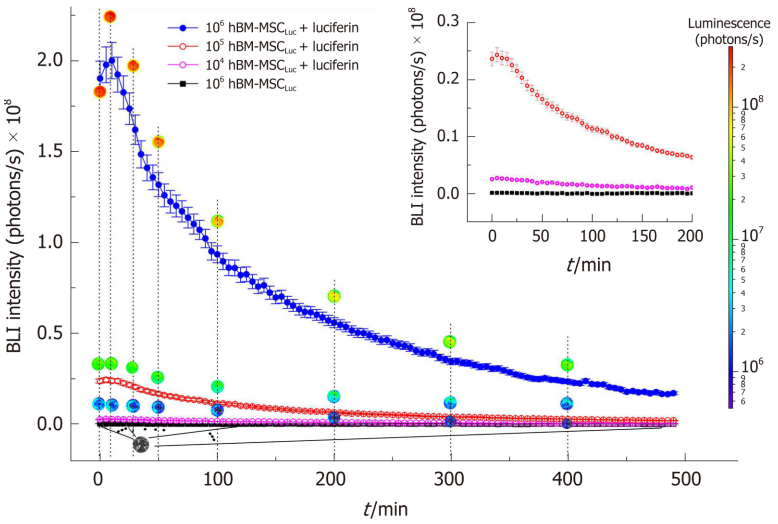

Figure 2 Expression of the bioluminescence signal as a function of number of human bone marrow mesenchymal stem cells$_{Luc}$ over 490 min. The 10^4, 10^5, and 10^6 hBM-MSC$_{Luc}$ groups with luciferin addition and the 10^6 hBM-MSC$_{Luc}$ group without luciferin addition are represented by curves in pink, red, blue and black, respectively. The inset shows the amplified signals of 10^4 and 10^5 hBM-MSC$_{Luc}$ with luciferin addition and 10^6 hBM-MSC$_{Luc}$ without luciferin addition. hBM-MSC: Human bone marrow mesenchymal stem cells.

increase in the MNP-IR750 concentration, due to the viability effect described above (Figure 5D).

Quantification of MNP-IR750 internalized by hBM-MSC$_{Luc}$ via MRI, ICP-MS and NIRF

Figure 6 shows the quantification of the iron load determined by using the MRI, ICP-MS and NIRF techniques. The process of quantification of the iron content internalized by hBM-MSC$_{Luc}$*via* MRI starts with relaxometry characterization, to determine the r^2 relaxivity of MNP-IR750 obtained upon T2-weighted image analysis (Figure 6A). The decay curves of the phantom signal related to the different concentrations of MNP-IR750 were obtained from of the ROI images shown in Figure 6A-I under the different TEs tested. The image obtained under the highest concentration of MNP-IR750 that is shown (Figure 6A-II) exhibited greater hypointensity in comparison with the control image; the gray image variations were proportional to the iron concentrations in the ROI, due to magnetic perturbation produced by the superparamagnetic properties of MNP-IR750.

The data adjustment of the relaxation rate as a function of the iron concentration (Figure 6A) followed a directly proportional straight line, which resulted in the r^2 angular coefficient value of (20.6 ± 1.4) × 10^{-4} μg Fe^{-1} ms^{-1} mL when adjusted by the method of least squares. The obtained r^2 value was characteristic of MRI contrast studies based on T2-weighted images using a 3T scanner.

Figure 6B shows the T2-weighted MRI signal intensity curves as a function of TE samples containing hBM-MSC$_{Luc}$ labeled in different concentrations of MNP-IR750. The curve decay was proportional to the iron load internalized by hBM-MSC$_{Luc}$. The T2 values of each sample were obtained from the adjustment of the MRI signal exponential decay curves, as shown in Figure 6B-IV. These values matched the MRI image of the ROI (Figure 6B-III) and were inversely proportional to the MNP-IR750 concentrations used for cellular labeling.

The MNP-IR750 load internalized by hBM-MSC$_{Luc}$ was determined from the obtained T2 values (Figure 6B, C) and r^2 values (Figure 6A) with equation 1. The number of MNP-IR750 per cell was calculated from the MNP-IR750 load using equation 2; these values were determined *via* the quantification of each labeling concentration, as shown in Table 1. The observed internalized MNP-IR750 loads $m_{cell}([Fe])$ as a function of the labeling concentration ([Fe]) were plotted and adjusted in an exponential curve, as shown in Figure 6C, following equation 3:

(3) $m_{cell}([Fe]) = m_{cell}^{max} \times (1\text{-}e^{-[Fe]/\varphi})$

where m_{cell}^{max} is the maximum number of MNP-IR750 that could be internalized by hBM-MSC$_{Luc}$ during the labeling process, and φ is a constant equivalent to the adequate MNP-IR750 concentration for achieving 63% of m_{cell}^{max} after cellular internalization. The obtained values of m_{cell}^{max} and φ are shown in Table 1, (m_{cell}^{max} = 7.91 ± 0.22 pg Fe/mL and φ = 14.46 ± 1.69 μg Fe/mL).

To verify the MRI quantification results, standard ICP-MS quantification was performed, as shown in Figure 6D. The MNP-IR750 load internalized by hBM-MSC$_{Luc}$

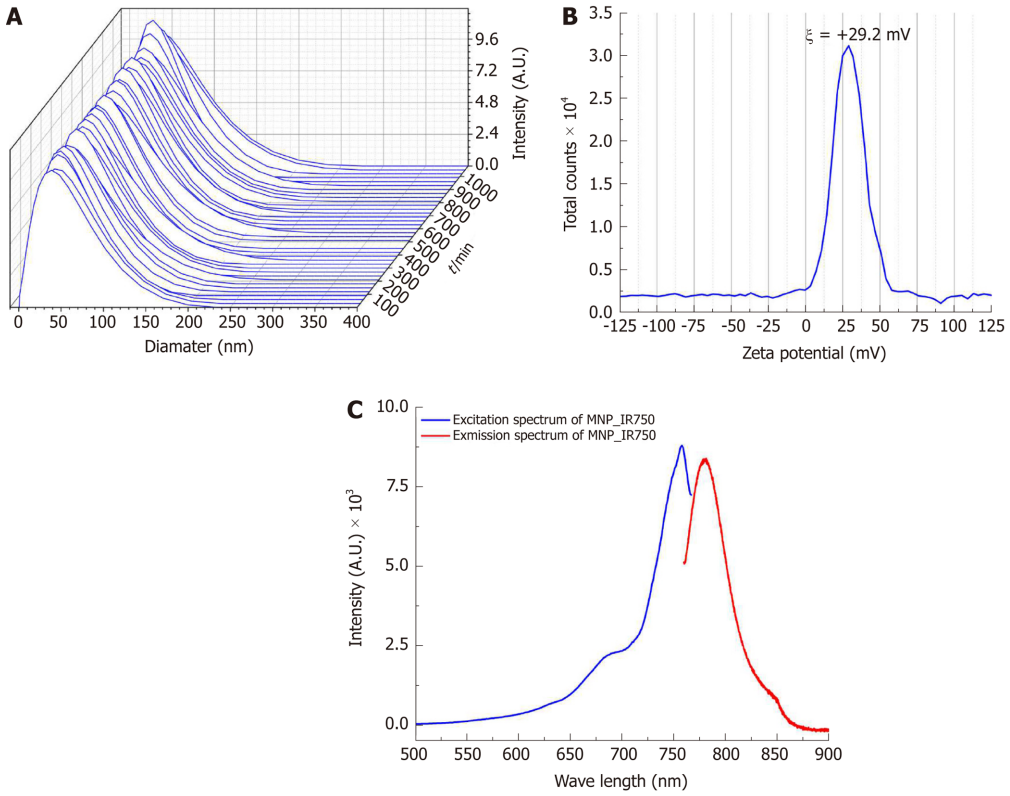

Figure 3 Characterization of the hydrodynamic diameter, zeta potential and optical properties of multimodal nanoparticles-IR750. A: Curves of the hydrodynamic size distribution of MNP-IR750 over 18 h; B: Spectrum of the surface charge of MNP-IR750 with a zeta potential at pH 7.4 of ξ = +29.2±1.9 mV; C: MNP-IR750 excitation/emission spectrum (blue and red curves, respectively), showing fluorescence intensity peaks of 757.9 and 779.4 nm, respectively. MNP: Multimodal nanoparticles.

was determined from the calibration curve generated using known MNP-IR750 concentrations, as depicted in Figure 6D,E, in which the adjustment curve presented correlation coefficient of R = 0.99. The number of MNP-IR750 internalized by hBM-MSC$_{Luc}$ at each labeling concentration was determined from the MNP-IR750 load internalized by hBM-MSC$_{Luc,}$ as shown in Table 1. m_{cell}^{max} = 7.91 ± 0.22 pg Fe/mL and φ = 14.46 ± 1.69 µg Fe/mL were determined from equation 3, as shown in Table 1.

The determination of the load and number of MNP-IR750 internalized by hBM-MSC$_{Luc}$*via* NIRF (Figure 6E) followed the same procedure used for ICP-MS after the calibration curve was generated (Figure 6E, F, R = 0.97). The values obtained for each MNP-IR750 concentration are shown in Table 1, along with the values adjusted based on an exponential curve with equation 3 (m_{cell}^{max} = 7.93 ± 0.40 pg Fe/mL and φ = 18.90 ± 2.14 µg Fe/mL).

The analysis of the correlation of the results regarding the MNP-IR750 load internalized by hBM-MSC$_{Luc}$ between the MRI, ICP-MS and NIRF techniques showed the same correlation coefficient of 0.99 (Figure 6F, blue dots for the correlation of ICP-MS - NIRF; green dots for the correlation of ICP-MS - MRI; and pink dots for the correlation of NIRF - MRI). The adjustment of the three correlation analyses is shown in Figure 6F (red dots).

Evaluation of the sensitivity of BLI, NIRF, and MRI signals of labeled hBM-MSC$_{Luc}$ implanted in animals

The evaluation of BLI, NIRF, and MRI signals *in vivo* and *ex vivo* after labeled hBM-MSC$_{Luc}$ were implanted in the animals in experiment 1 showed sensitivity in the detection of MNP-IR750 at concentrations of 5, 20 and 50 µg Fe/mL (Figure 7), after 4 h of cell implantation.

A BLI signal acquired after the implantation of the hBM-MSCLuc was present in all groups (S_control, S5, S20, and S50), even in the control group (1.31 ± 0.11; 10^7 photons/s), in which the implanted cells were not labeled with MNP-IR750 (Figure 7A-D and Figure 8J). The intensity of the BLI signal showed low variability in the S5 (1.36 ± 0.12) 10^7, S20 (1.23 ± 0.11) 10^7, and S50 (1.21 ± 0.10) 10^7 groups in relation to the increase in the MNP-IR750 concentrations (Figure 7 B-D), without any significant difference between all sham groups analyzed at each MNP-IR750 concentration (Figure 8J, *P* = 0.392).

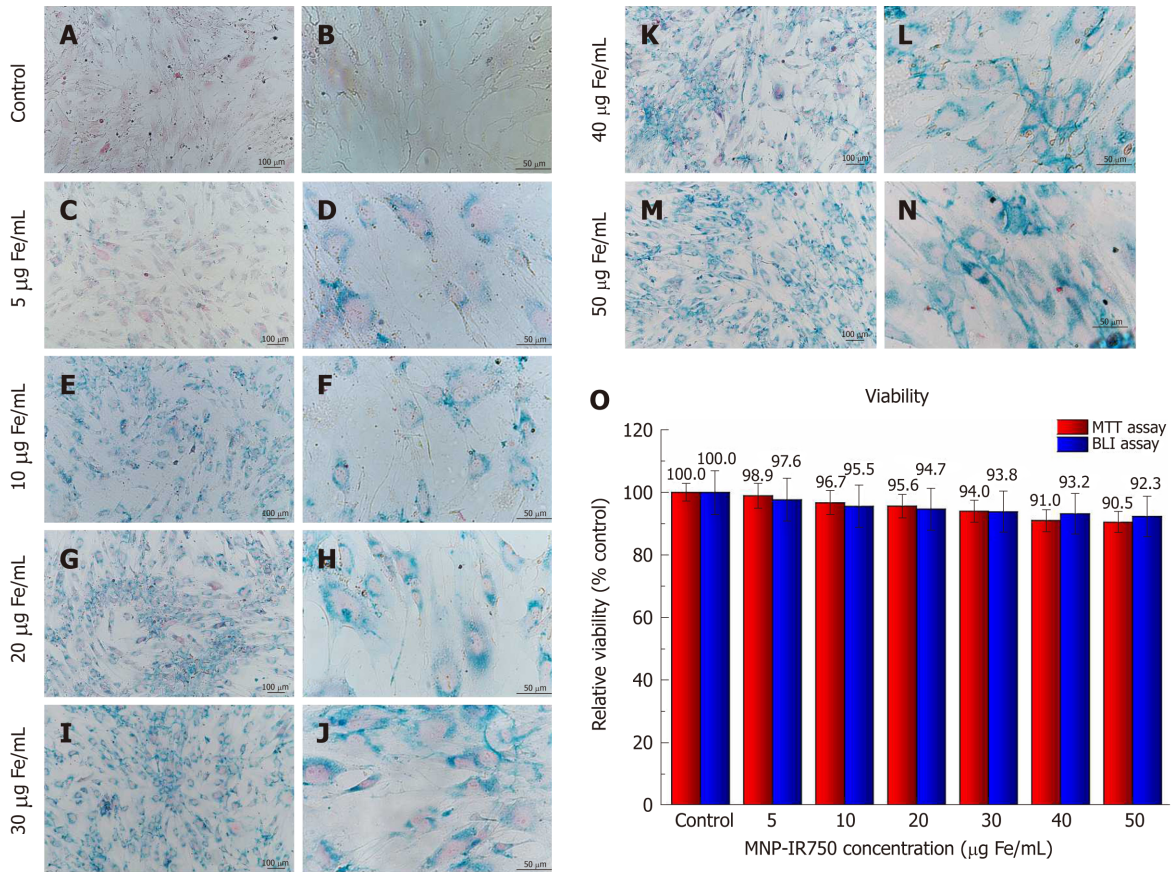

Figure 4 Internalization and viability analysis of human bone marrow mesenchymal stem cells$_{Luc}$ labeled with multimodal nanoparticles-IR750. A-N: Optical microscopy images of hBM-MSC$_{Luc}$ labeled with MNP-IR750, shown at 10 × (left column images) and 40 × (right column images); O: Cellular viability of hBM-MSC$_{Luc}$ after labeling in MTT (red bars) and BLI (blue bars) assays. Internalization of MPN-IR750 was performed at the following concentrations: 5, 10, 20, 30, 40 and 50 µg Fe/mL. hBM-MSC: Human bone marrow mesenchymal stem cells; MNP: Multimodal nanoparticles; MTT: The 3-[4,5-dimethylthiazol-2-yl]-2,5 diphenyl tetrazolium bromide; BLI: Bioluminescent images.

The NIRF signal was detected in the S5 (1.09 ± 0.19) µg Fe, S20 (3.10 ± 0.50) µg Fe and S50 (5.80 ± 0.73) µg Fe groups. A significant difference between MNP-IR750 concentrations was found *via* the ANOVA test, with a P value < 0.001(Figure 8H), where the increase in the NIRF intensity signal was proportional to the increase in the nanoparticle concentration (Figure 7 F-H). In the *ex vivo* evaluation, the NIRF signal was also detected and remained in the same brain region indicated in the *in vivo* NIRF examination (Figure 7 I-L). This evaluation also showed the same behavior with regard to intensity, but with high evidence of contrast (Figure 7 J-L), due to the decreased attenuation caused by the presence of tissue in *in vivo* images. The NIRF signal was not detected in the S_control group when evaluated *in vivo* (Figure 7E) or *ex vivo* (Figure 7I)

The *ex vivo* MRI intensity signal showed sensitivity in the detection of MNP-IR750 at different concentrations (Figure 7 M-T and Figure 8H), due to the magnetic properties of these nanoparticles. The values for each group were as follows: S5 (0.30 ± 0.15) µg Fe, S25 (1.10 ± 0.32) µg Fe and S50 (5.20 ± 0.78) µg Fe, and a significant difference was found in the comparison between them (P < 0.001). The post hoc test showed no difference between the S5 and S20 groups (P = 0.254), as shown in sagittal (Figure 7P) and coronal slices (Figure 7T). However, a more remarkable difference was revealed when comparing S50 with S5 or S20, and this difference remained significant after the post hoc test (P < 0.001), as shown in graphic representation of Figure 8H.

When the intensity quantification results were compared between techniques, a significant difference was detected between the NIRF and MRI results in the S5 and S25 groups (P = 0.005 and P = 0.004, respectively), as shown in Figure 8H.

Evaluation of the sensitivity of NIRF, BLI and MRI signals of labeled hBM-MSC$_{Luc}$ implanted in animals subjected to stroke induction

Before cellular implantation, a focal ischemic lesion induced by thermocoagulation (stroke induction) was confirmed from local blood perfusion images, which showed a

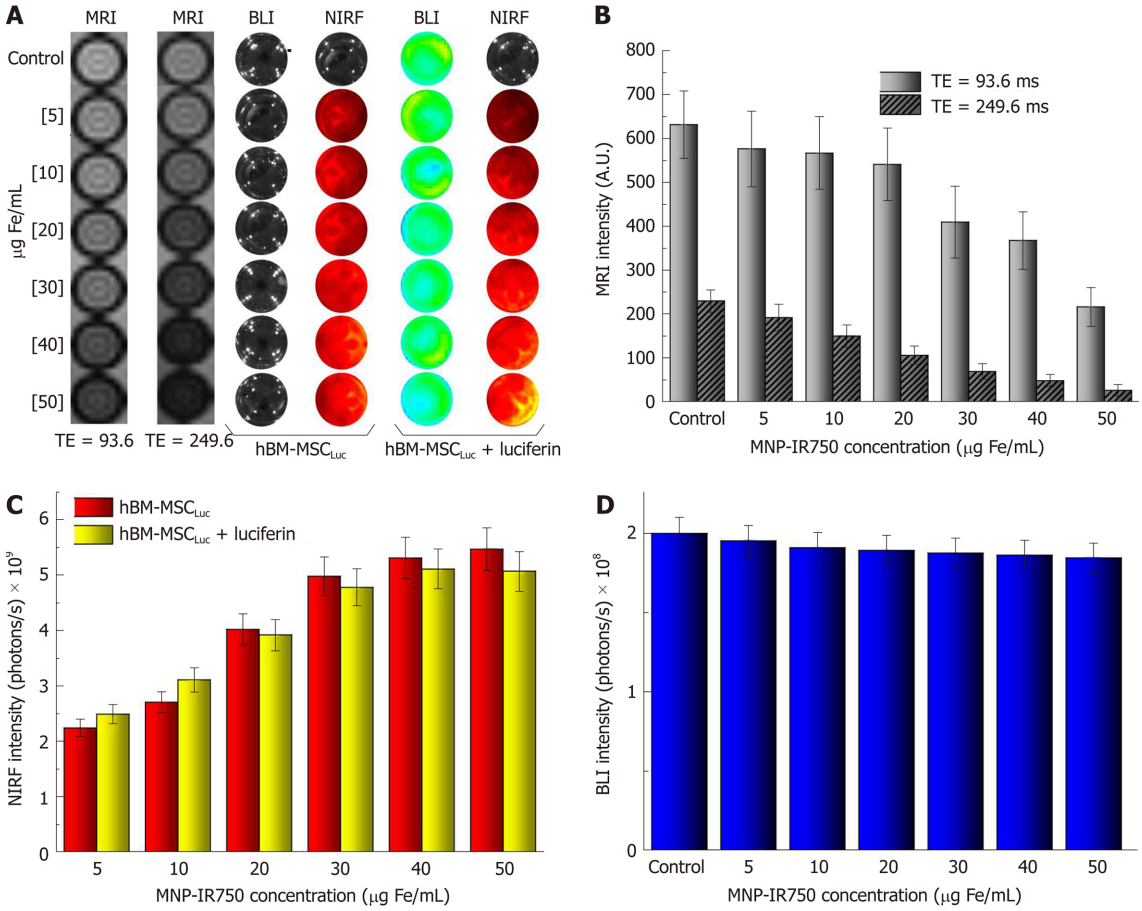

Figure 5 Evaluation of magnetic resonance imaging, near-infrared fluorescence and bioluminescent images intensity signals *in vitro*. A: Images of hBM-MSC$_{Luc}$ phantoms, labeled with different concentrations of MNP-IR750, comparing short *vs* long TEs *via* MRI and before *vs* after the addition of luciferin *via* NIRF and BLI; B: Graphic representation of the MRI signal intensity of all samples acquired with a TE of 93.6 ms (light gray bars) and a TE of 249.6 ms (dark gray bars); C: Graphic representation of the NIRF signal intensity of all samples acquiring before luciferin addition (red bars) and after luciferin addition (yellow bars); D: Graphic representation of BLI signal intensity after luciferin addition in all samples with different concentrations of MNP-IR750. hBM-MSC: Human bone marrow mesenchymal stem cells; MNP: Multimodal nanoparticles; MRI: Magnetic resonance imaging; NIRF: Near-infrared fluorescence; BLI: Bioluminescent images.

decrease in the local blood flow intensity between the basal image and the image acquired after 30 min of induction (Figure 8-I). This blood perfusion decrease represented graphically revealed a reduction of 75% ± 5% between the basal measurement and that performed after 30 min of induction (Figure 8 II). TTC staining performed 120 min after ischemic lesion induction complemented the blood perfusion analysis and showed an ischemic lesion in the pale area (non-TTC-stained) of the left sensorimotor cortex, extending to the corpus callosum and the subcortical brain region in the stroke group compared to the sham group, where the latter was only subjected to the craniectomy procedure (Figure 8 III).

The BLI intensity was found to decrease significantly in the sham_50 group (P < 0.001; Figure 8J) when the intensity of the image acquired at 4 h (1.21 ± 0.10) 10^7 (Figure 7D, J) was compared to that at 6 d after cell implantation (0.12 ± 0.07; 10^7 photons/s) (Figure 8AJ), with the same nanoparticle concentration in both groups. However, after 6 d of cell implantation, the stroke_50 group showed a significantly high signal intensity (3.02 ± 0.12; 10^7 photons/s) (Figure 8D, J) in relation to the sham_50 group (0.12 ± 0.07; 10^7 photons/s) in experiment 2 (P < 0.001; Figure 8A, J).

The NIRF and MRI images also showed a significant intensity reduction in the sham_50 group (P < 0.001; Figure 7H, L, P, T and 8B, C, E-H) when the two acquisition times were compared (4 h and 6 d) under the same nanoparticle concentration. Additionally, significant intensity increase was observed after 6 d of cell implantation under both techniques when the sham_50 group was compared to the stroke_50 group (P = 0.004 and P < 0.001, respectively; Figure 8H). The NIRF image intensity between times of acquisition was reduced from 5.80 ± 0.73 μg Fe in the S50 group (Figure 7H and Figure 8H) to 1.30 ± 0.21 μg Fe in the sham_50 group (Figure 8B, H), and the MRI intensity decreased from 5.20 ± 0.78 μg Fe in the S50 group (Figure 7P, T and Figure 8H) to 0.01 ± 0.01 μg Fe in the sham_50 group (Figure 8C, H). Regarding the difference between the sham and stroke groups at the same

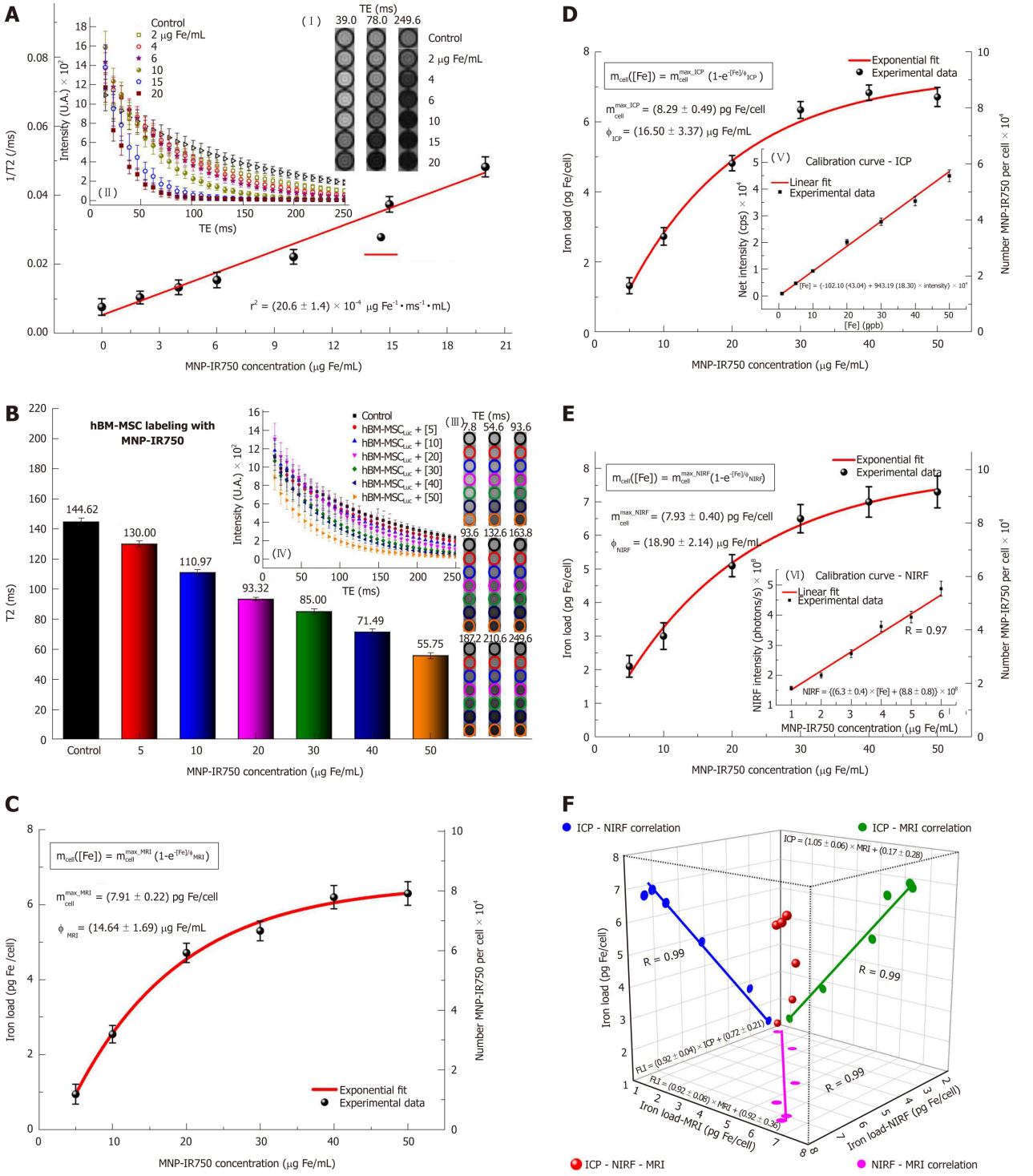

Figure 6 Quantification of multimodal nanoparticles-IR750 internalized by human bone marrow mesenchymal stem cells$_{Luc}$ using magnetic resonance imaging, inductively coupled plasma-mass spectrometry and near-infrared fluorescence images *in vitro*. For quantification *via* MRI, (A) the r_2 values were determined from the intensity signal of MNP-IR750 at different concentrations as a function of TEs (I-II); B: the T2 values of hBM-MSC$_{Luc}$ labeled with MNP-IR750 at different concentrations were determined based on the adjustment of the MRI signal exponential decay curves obtained for the MRI images of ROIs (III-IV); C: the MNP-IR750 load and number internalized per cell as a function of different labeling concentrations were determined *via* MRI, and these values were adjusted based on an exponential curve, following equation 3 and the parameters determined for this equation; D: the MNP-IR750 load and number internalized per cell as a function of different labeling concentrations were determined *via* ICP-MS (V) from the calibration curve generated using known MNP-IR750 concentrations, and the values determined *via* ICP-MS quantification were adjusted based on an exponential curve, following equation 3 and the parameters determined for this equation; E: the MNP-IR750 load and number internalized per cell as a function of different labeling concentrations were determined *via* NIRF imaging (VI) from the calibration curve generated using known MNP-IR750 concentrations, and the values determined *via* NIRF quantification were adjusted with an exponential curve, following equation 3 and the parameters determined for this equation; and F: the correlation of the MNP-IR750 load internalized by hBM-MSC$_{Luc}$ was compared between ICP-MS and NIRF (blue dots), ICP-MS and MRI (green dots), NIRF and MRI (pink dots). hBM-MSC: Human bone marrow mesenchymal stem cells; MNP: Multimodal nanoparticles; ICP-MS: Inductively coupled plasma-mass spectrometry; MRI: Magnetic resonance imaging; NIRF: Near-infrared fluorescence; BLI: Bioluminescent images.

Table 1 Quantification of the multimodal nanoparticles-IR750 load and number internalized by human bone marrow mesenchymal stem cells$_{Luc}$ *via* magnetic resonance imaging, inductively coupled plasma-mass spectrometry magnetic resonance imaging and near-infrared fluorescence

[Fe] in cell labeling (μg Fe/mL)	&Iron load /cell (pg Fe/mL)		
	¥[Number MNP-IR750 per cell × 10^4]		
	MRI	**ICP-MS**	**NIRF**
[5]	&0.94 ± 0.26	&1.32 ± 0.23	&2.12 ± 0.32
	¥1.19 ± 0.34	¥1.66 ± 0.28	¥2.64 ± 0.41
[10]	&2.54 ± 0.23	&2.73 ± 0.25	&3.02 ± 0.39
	¥3.20 ± 0.29	¥3.43 ± 0.31	¥3.77 ± 0.49
[20]	&4.71 ± 0.25	&4.82 ± 0.21	&5.14 ± 0.33
	¥5.92 ± 0.32	¥6.06 ± 0.26	¥6.41 ± 0.41
[30]	&5.31 ± 0.26	&6.34 ± 0.24	&6.52 ± 0.42
	¥6.66 ± 0.33	¥7.97 ± 0.30	¥8.17 ± 0.53
[40]	&6.20 ± 0.31	&6.83 ± 0.22	&7.12 ± 0.46
	¥7.79 ± 0.38	¥8.58 ± 0.27	¥8.79 ± 0.57
[50]	&6.30 ± 0.32	&6.71 ± 0.28	&7.3 ± 0.47
	¥7.92 ± 0.39	¥8.43 ± 0.35	¥9.17 ± 0.59
	Parameter fit curve		
	$m_{cell}([Fe]) = m_{cell}^{max} \times (1\text{-}e^{-[Fe]/\varphi})$		
Parameter	**MRI**	**ICP-MS**	**NIRF**
m_{cell}^{max} (pg Fe/mL)	7.91 ± 0.22	8.29 ± 0.49	7.93 ± 0.40
φ (μg Fe/mL)	14.64 ± 1.69	16.50 ± 3.37	18.90 ± 2.14

MRI: Magnetic resonance image; ICP-MS: Inductively coupled plasma - mass spectrometry; NIRF: Near-infrared fluorescence; $m_{cell}([Fe])$: MNP-IR750 load values internalized as a function of the labeling concentration; m_{cell}^{max}: maximum number of MNP-IR750 that could be internalized by hBM-MSC$_{Luc}$; φ: Constant equivalent of the adequate MNP-IR750 concentration for achieving 63% of m_{cell}^{max} after the cellular internalization process.

time point (6 d after cell implantation), the NIRF intensity increased from 1.30 ± 0.21 μg Fe in the sham_50 group (Figure 8B, H) to 2.80 ± 0.45 μg Fe in the stroke_50 group (Figure 8E,H), and the *ex vivo* MRI results increased from 0.01 ± 0.01 μg Fe in the sham_50 group (Figure 8C, H) to 3.20 ± 0.48 μg Fe in the stroke_50 group (Figure 8F-H). Figure 8F (yellow arrow) shows only an image of the stroke lesion, and the MRI hypointense image is indicated with red arrows in Figures 7N-P and 8F, G.

When the intensity quantification results were compared between techniques in experiment 2, a significant difference was detected between the NIRF and MRI results in the sham_50 group ($P < 0.001$), as shown in Figure 8H.

DISCUSSION

Although meta-analyses have examined the benefits of cell transplantation in experimental stroke[23], the low viable cell retention after transplantation in ischemic brain areas still represents the major obstacle to the successful clinical translation of cell-based stroke repair approaches. The present study showed high hBM-MSC viability upon transfection with luciferase and labeling with multimodal nanoparticles. These specific nanoparticles exhibit biocompatibility, magnetic and NIRF properties and a high positive zeta potential, which favors viability. The results further showed sensitivity in triple-image evaluations (MRI, BLI and NIRF), highlighting the importance of quantification of the MNP-IR750 load internalized by cells when different concentrations are used in *in vitro* analyses for application to *in vivo* analysis. These findings demonstrated effectiveness of signal detection under the triple-image modality with the highest concentration tested, as an approach for cellular therapy in a stroke lesion model.

Stem cells exhibit remarkable applicability in cellular therapy for drug discovery and regenerative medicine. Moreover, this type of therapy has increased the effectiveness of this approach when associated with noninvasive image modalities,

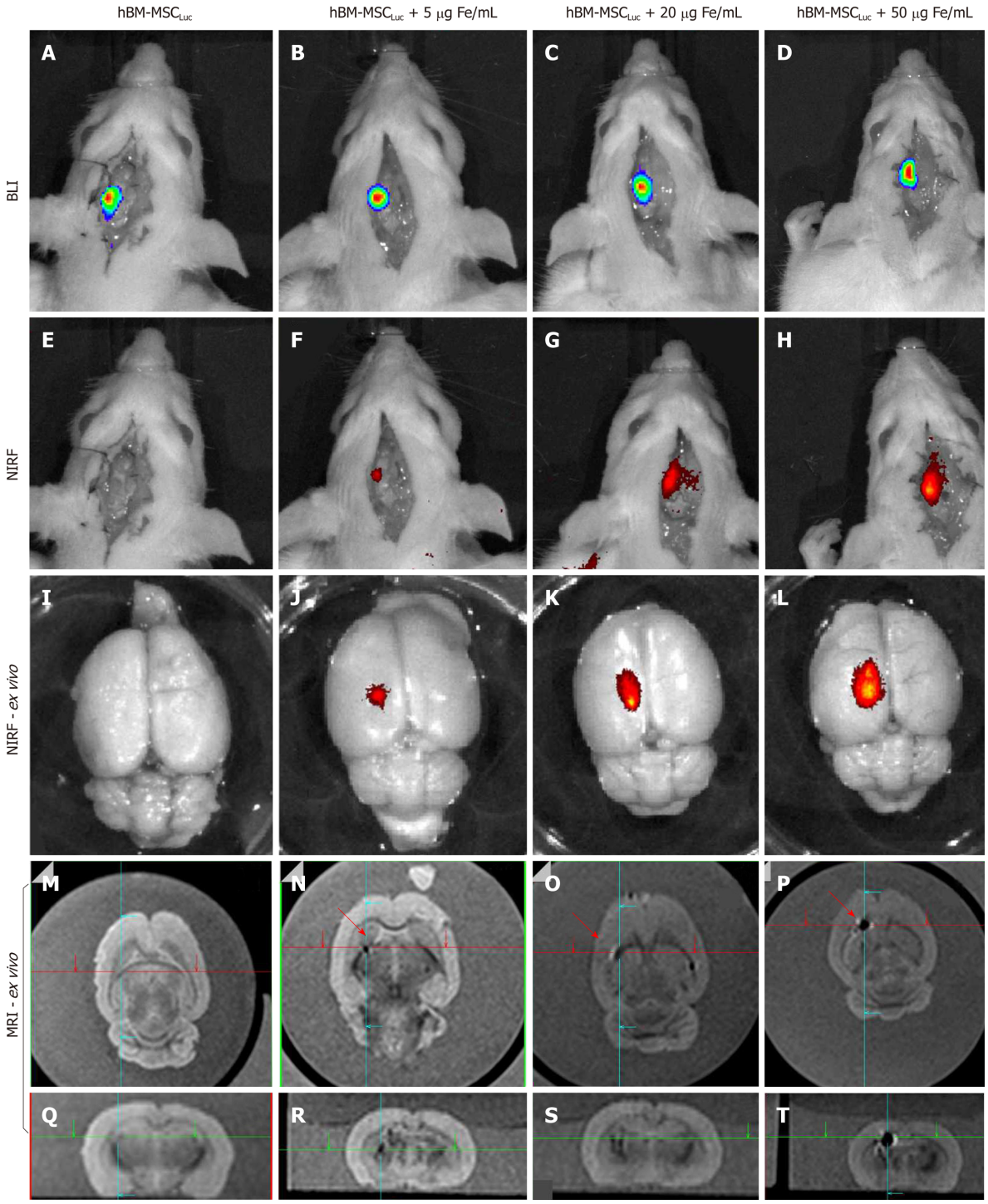

Figure 7 Evaluation of bioluminescent images, near-infrared fluorescence, and magnetic resonance imaging signals of labeled human bone marrow mesenchymal stem cells$_{Luc}$ implanted in animals (sham groups). A: BLI image of the sham_control group after luciferin addition; B-D: BLI images after luciferin addition in the sham_S5, sham_S20 and sham_S50 groups; E: NIRF image of the sham_control group; F-H: NIRF images of the sham_S5, sham_S20 and sham_S50 groups; I, L: *ex vivo* NIRF images of all groups; M-Q: Sagittal and coronal MRI of the sham_control group; N-P: Sagittal MRI of the sham_s5, sham_s20 and sham_S50 groups, showing the position of iron signal detection with red arrows; R-T: Coronal MRI of the sham_s5, sham_s20 and sham_S50 groups, showing the position of iron signal detection with crossing green lines. (n = 7 rats/group). BLI: Bioluminescent images; hBM-MSC: Human bone marrow mesenchymal stem cells; NIRF: Near-infrared fluorescence; MRI: Magnetic resonance imaging.

providing complementary information through the evaluation of cellular viability, the state of differentiation, cell numbers, cell tracking and cell fate. This approach also provides information about the behavior and function of stem cell protein expression levels and interactions between the cells and adjacent tissue[24].

It is important to select an appropriate imaging approach, taking into account factors such as the application, the experimental subject under study, and the goal of the experiment. The combined image modalities have improved the accuracy of

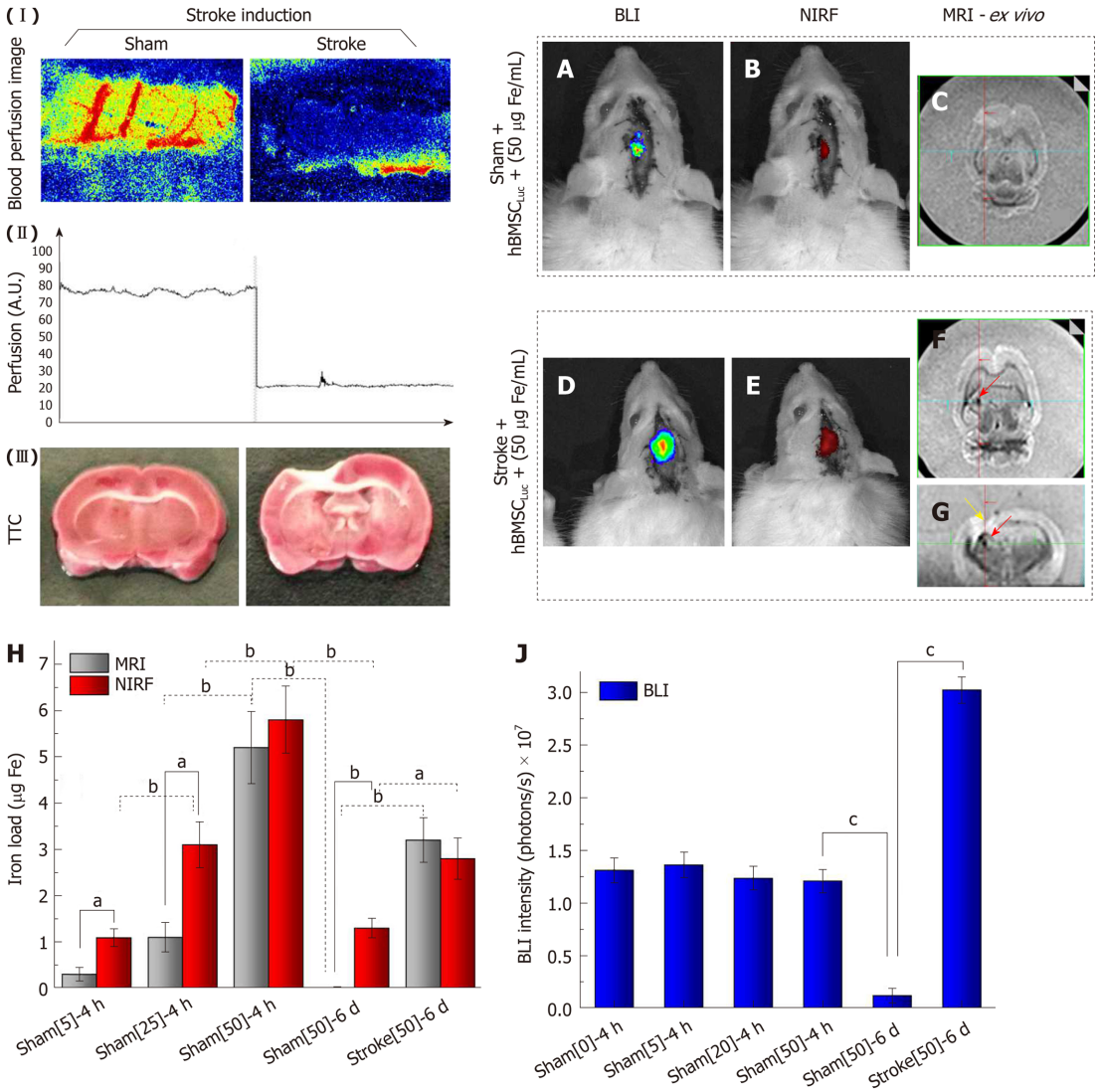

Figure 8 Evaluation of near-infrared fluorescence, bioluminescent images (*in vivo*) and magnetic resonance imaging signals (*ex vivo*) after 6 d of stroke induction. (I) Local blood perfusion images of the basal condition and 30 min after stroke induction by thermocoagulation; (II) graphic representation of local blood perfusion showing the decrease in perfusion from 80 to 20 au, comparing the basal condition to 30 min after stroke induction; (III) TTC staining of the sham and stroke groups performed 120 min after ischemic lesion induction; A, B: *In vivo* BLI and NIRF images of the sham_50 group; C: *Ex vivo* MRI results of the sham_50 group; D, E: *In vivo* BLI and NIRF images of the stroke_50 group; F, G: *Ex vivo* MRI results of the stroke_50 group (red arrows show the presence of nanoparticles, and a yellow arrow shows the stroke lesion); H: Graphic representation of quantification of the iron load *via* NIRF (red bars) and MRI (gray bars) in different groups in experiments 1 and 2, $^aP < 0.05$, $^bP < 0.001$, MRI *vs* NIRF; J: Graphic representation of BLI intensity (blue bars) in different groups in experiments 1 and 2, $^cP < 0.05$, *vs* sham[50]-6 d ($n = 7$ rats/group). BLI: Bioluminescent images; NIRF: Near-infrared fluorescence;

cellular therapy by using advanced technology to develop new hybrid tracers (multicomponent nanoparticles) containing two or more imaging contrast agents that permit several imaging techniques to be used in a hybrid manner, which is also known as multimodal imaging[25].

Dual-image modalities are often used in *in vivo* studies for homing and tracking evaluations under different approaches[10,26,27]. However, triple-image modality analyses, such as the analysis performed in this study, are currently scarce in the literature, and such analyses require multimodal nanoparticles. In our study, the nanoparticles exhibited near-infrared fluorescence and magnetic properties associated with stem cell transfection with luciferase. The NIRF nanoparticle properties showed excitation/emission fluorescence intensity peaks of 757.9 and 779.4 nm, respectively, which correspond to the NIR wavelength range specified by the manufacturer. NIR molecular probes offer two major advantages over those that emit visible wavelengths for *in vivo* analyses: lower absorption of biological tissues compared to visible light, allowing photon penetration through tissue to assess deeper structures; and a high signal/noise ratio, which minimizes the effects of tissue autofluorescence[28].

The magnetic nanoparticle properties showed good contrast in T_2-weighted images due to r^2 relaxivity characteristics, which depend on temperature, magnetic field

intensity and the size, composition, concentration, magnetic moment, aggregation, and coating of nanoparticles[29]. The T_2-weighted MRI intensity signals of the samples showed dark images in the presence of MNP-IR750. Therefore, high nanoparticle concentrations lead to a high local inhomogeneity field, decreasing the intensity signal and resulting in short T_2 values[10]. The r^2 value of 115.1 ± 8.0 $mm^{-1}s^{-1}$ obtained for MNP-IR750 is in accord with that of other commercial nanoparticles, such as feridex (size = 62 nm) and Resovist (size between 80 and 180 nm), which present r^2 values of 93 and 143 Mm-1s-1, respectively, correlated with the hydrodynamic size of these nanoparticles[30]. Thus, MNP-IR750 internalized in hBM-MSC_{Luc} presents high potential as a contrast agent for T_2-weighted MRI.

Among the lines of stem cells used in therapeutic approaches, MSCs present remarkable characteristics as neuronal markers *in vivo* as well as trophic factors such as brain-derived neurotrophic factor (BDNF), glial-derived neurotrophic factor (GDNF), VEGF, neurotrophin-3 (NT3), and fibroblast growth factor (FGF), in addition to thrombospondins released by these cells in response to the local microenvironment. These factors, associated with neurogenesis stimulation and angiogenesis immunomodulation, promote functional recovery[31]. These stem cells also stimulate astrocytes, which were used as a therapeutic target in the past because of their roles in maintaining neuronal function and effective endogenous repair.

Other relevant aspects of hMSCs relevant to their application in cellular therapy are their multipotency, biological characteristics, repair capacity, immunosuppressiveness, ease of isolation and expansion, and safety, without any possibility of malignant transformation after the infusion of allogeneic cells[32]. Bone marrow has been the major source of these cells, which directed the choices we made in this study.

The collection, isolation and immunophenotypic profiling of hBM-MSCs showed adequate results, confirming high levels of MSC markers (above of 93%) and low levels or absence of hematopoietic markers (below 3%) and leukocyte antigens. Such results are compatible with other studies on the same topic[33,34].

The nanoparticles tested showed a polydispersed size distribution and an average hydrodynamic diameter of 38.2 ± 0.5 nm, compatible with the manufacturer's specifications. They also showed adequate stability in DMEM-LG culture supplemented with 10% PBS over 18 h (time of incubation with the cells), avoiding agglomeration of nanoparticles, which may occur due to their interaction with the protein-supplemented and electrolyte-rich cell culture medium[35]. Another observed advantage was maintenance of the equilibrium of existing forces involved in the interaction between nanoparticles, such as electrostatic forces, Van der Waals forces, steric forces, and magnetic forces modulated *via* the Brownian motion associated with nanoparticles[35,36].

Another important aspect of the physical-chemical properties of nanoparticles in the cellular internalization process during nanoparticle uptake by cells is the electrophoretic mobility capacity of nanoparticles (zeta potential)[37]. Cells exhibit greater uptake of nanoparticles with a positive charge compared to those with a negative charge, which might be attributed to the attractive interaction between the negatively charged cell membrane and positively charged nanoparticles[38]. This phenomenon was a relevant factor in our study, due to the use of nanoparticles with a positive zeta potential of ξ = +29.2 ± 1.9 mV.

However, studies have demonstrated that shape, size and surface charge substantially influence nanoparticle internalization by cells[38,39]. Studies that have used nanoparticles with a negative zeta potential or a low positive zeta potential have included strategies for facilitating the internalization process, such as the use of transfection agents (poly(L-lysine) - PLL, protamine sulfate lipofectamine, among others)[40,41] or physical strategies (static or dynamic magnetic field) [42,43].

After labeling the cells with nanoparticles without any strategy for facilitating the internalization process, it was possible to verify that the use of nanoparticles with a positive zeta potential provided efficient labeling from the lowest nanoparticle concentrations to the highest concentration, based on Prussian blue staining. It was also possible to maintain the cellular morphological characteristics shown in optical microscopy images. Cellular viability assessed *via* MTT and BLI analyses was above 90% in all tested concentrations of nanoparticles, which varied from 0 to 50 μg Fe/mL. The same nanoparticle composition, with the exception of the type of fluorophore (rhodamine), resulted in little difference in cellular viability when assessed in the same range of nanoparticle concentrations (100% to 95%) using the MTT assay. However, a significantly high apoptosis rate was found in 100 μg Fe/mL (78% viability) in comparison to unlabeled cells, due to the toxic effect of a high concentration on stem cell viability[26,27,44]. A study by Addicott (2010) also showed that these nanoparticles maintained the immunophenotypic profile, even after labeling of hBM-MSCs[44].

Quantification of the nanoparticle load in cells *via* different imaging modalities (BLI, MRI and NIRF) provides indirect measurements of the load. Complementary analysis with ICP-MS has been performed in parallel in correlation analyses between indirect and direct measurements of nanoparticle load[10].

By analyzing the quantification results of the iron load/cell in different nanoparticle concentrations using MRI, ICP-MS and NIRF (Table 1), we could verify that the quantification of the iron load/cell *via* NIRF was over-estimated in relation to the ICP-MS values, mainly in the lowest concentrations (61% and 11% higher for 5 and 10 μg Fe/mL, respectively, *vs* 7, 3, 4 and 9% higher for 20, 30, 40, and 50 μg Fe/mL concentrations, respectively). The MRI quantification values also varied in relation to the ICP-MS values, but were underestimated at 29, 7, 2, 16, 9 and 6% for 5, 10, 20, 30, 40 and 50 μg Fe/mL, respectively, and the largest difference occurred in the lowest concentrations of nanoparticle tested (29% lower for 5 μg Fe/mL). This variability of results can be explained by a difference in sensitivity under each imaging modality, as MRI shows low sensitivity for small concentrations above 10^{-3} moles, whereas NIRF presents good sensitivity for ranges between 10^{-9} and 10^{-12} moles[45]. However, whether MRI and NIRF tracking of stem cells can reliably evaluate long-term cell engraftment and cell survival remains a controversial issue[46].

In this study, the maximum number of MNP-IR750 values adjusted based on an exponential curve showed values that were approximately 5% lower for MRI and NIRF in relation to ICP-MS. Under a constant value to achieve 63% of the maximum number of nanoparticles internalized, variations that were approximately 12% greater for NIRF and lower for MRI were detected in relation to ICP-MS values.

The correlation of the load quantification results based on images and spectrum techniques applied in our study *in vitro* (MRI, NIRF and ICP-MS) helped to improve the precision of these data and to understand the variation between the measurements according to the tested nanoparticle concentrations. Studies on multifunctional nanoparticles involving evaluations *via* multimodal images often show image analyses in a qualitative manner[26,27]. However, other studies either complement qualitative image analyses with techniques that permit nanoparticle quantification with more precision, such as inductively coupled plasma spectrometry[47,48], or use different approaches to quantify the nanoparticle load in cells by using image analysis[10,14,16]. However, none of these reported studies have included correlation analysis of the results obtained under each technique when applied in a quantitative way. This correlation could increase the accuracy of the obtained information, improving the interpretation of the analysis between the techniques as well as comparison with other studies. Therefore, the multimodal imaging analysis described above showed that MRI and NIRF presented a high correlation with ICP-MS, which is the *in vitro* gold standard for iron analysis[49]; the MRI results were lower than, while those of NIRF were greater than the ICP-MS results.

The sensitivity of triple-modal imaging was also analyzed *in vivo*. Experiment 1 showed that the NIRF and MRI signal intensity in the sham groups after 4 h of cell implantation was proportional to the tested nanoparticle concentrations (low, intermediate and high concentrations) and was constant in BLI images for all conditions analyzed. Experiment 2 also showed a difference in the triple-modal images between sham group and the stroke group after 6 d of cells implantation, using the same concentration of nanoparticles (50 μg Fe/mL of MNP-IR750), but in a different physiopathological process.

The BLI intensity results for experiment 1 showed little variability between the sham groups with labeled cells (S5, S20 and S50) and the sham group with unlabeled cells (S_control). This result was compatible with the decreased viability found in the *in vitro* study and corroborates other studies that have analyzed cell viability in the presence of similar nanoparticles at the same range of concentrations[26,27,44]. Considering cell viability under a high concentration of nanoparticles, experiment 2 showed maintenance of the BLI signal in both groups, even after 6 d of surgery procedures (craniectomy and stroke induction). The BLI intensity was high in the stroke_50 group, mainly near the stroke area, due to ischemic status, challenging the metabolic source for initiating the bioluminescence process[50]. The reduction of the BLI sign in the sham_50 group most likely resulted from the progressive biodistribution of grafted cells in the body[51].

Karp and Leng Teo[52] described MSC homing as "the arrest of MSCs within the vasculature of the respective tissue," followed by transmigration across the endothelium. These authors suggest that chemokines, cytokines, and growth factors released upon tissue injury provide migratory cues for stem cells implanted in a systemic or localized way. Concerning the homing capability of MSCs, many studies have indicated that systemically infused MSCs can migrate to injured, inflamed tissues and exert therapeutic effects[53]. Therefore, inflammation promotes chemotaxis of stem cells to the region of ischemia; this potential is initiated 24 h after injury and

stabilizes 5 to 7 d after ischemia, then decreases after 14 d[53]. Our results verified this reported kinetic observation, with *in vivo* bioluminescence images being found to be more intense after 6 d of lesion induction. Duan *et al*[46] verified the finding of significant chemotaxis of viable hBM-MSCs in ischemic areas.

Another optical image modality provided complementary information on both living and dead cells. NIRF intensity signal analysis *in vivo* showed high sensitivity in the detection of differences in nanoparticle concentrations, with an even greater difference being observed in *ex vivo* analysis (Experiment 1). These findings corroborate other studies that have indicated a strong linear relationship of signals with corresponding nanoparticle concentrations[14]. However, the signal was below the intensity detected in the *in vitro* study, due to the decreased attenuation caused by the presence of tissue[28]. Experiment 2 showed that the NIRF signal presented a good spatial resolution because MSCs were mainly concentrated at the injury site, with a small number of cells migrating to the periphery of the injury area; however, the NIRF signal decreased over time, due to exocytosis and cell division, thus diluting the signal in the target area[54].

The intensity of the MRI signal showed a remarkable region of hypointensity under the highest nanoparticle concentration, while similar results were found between the other lower concentrations, allowing good localization of cells labeled with SPIONs, due to the high structural resolution[27]. However, SPION-based MRI cannot provide reliable information on longitudinal viability and might overestimate the survival of SPION-labeled stem cells in other ischemic models. Duan *et al*[46] showed the dynamic changes in a low signal volume in MRI in a preclinical stroke model, due to a consistent pattern of change in the number of viable cells. Thus, MRI and NIRF present some challenges in the longitudinal monitoring of stem cells. Zhang *et al*[55] showed that cell grafts with SPION can be detected as a hypointense signal in T2 and T2* MRI imaging up to 6 wk after implantation; a few viable stem cells and many grafted cells that differentiate into astrocytes at 6 wk are observed. These results suggest that the iron-dependent signal in T2*-weighted imaging can lead to overestimation of the real number of viable cell grafts. Considering that the number of transplanted stem cells that home and survive in host organs in the first several h is generally very low[56], the gradual reduction in graft size most likely results from the progressively decreased survival of grafted cells. The histological data showed many extracellular iron particles and microglia/macrophages present at the implantation site at 6 wk. Therefore, the longitudinal cell viability observed *via* NIRF might represent overestimated data. The accuracy of such data can be affected by many factors, especially by cell death and concomitant microglia/macrophage accumulation potentially activated by immunoreaction. Thus, the biodistribution, proliferation and differentiation of transplanted cells decreases the NIRF signal over time and might result in overestimation, as observed for the MRI signal.

The BLI signal analyzed in the stroke model after cell therapy remained constant until 28 d after stroke induction, but disappeared after 6 d in the sham group. It has also been reported that 28 d after induction, the intensity of the BLI signal is significantly higher than following other implantations performed earlier (after 2 h or 1 wk of stroke induction)[51]. The reduction of the BLI sign observed in the sham group most likely resulted from the progressive biodistribution of grafted cells in the body. Our results showed that the stem cells were viable, even in a challenging microenvironment, due to a lack of O_2 and adenosine triphosphate (ATP), 6 d after ischemia induction. In conclusion, cell implantation is advised soon after stroke induction to increase the efficiency of cellular therapy monitored *via* the BLI signal.

Finally, we demonstrated that MNP-IR750 could be used to monitor cell grafts noninvasively, longitudinally, and repetitively, enabling the assessment of cell graft conditions *in vivo* after stroke for multimodal imaging assessment. The BLI signal of hBM-MSC_{Luc} showed the best imaging technique for functional and longitudinal assessment. The applicability of multimodal imaging should always be analyzed in accordance with the limitations and advantages of each technique involved.

ARTICLE HIGHLIGHTS

Research background

Mesenchymal stem cells (MSCs) have been widely tested for therapeutic efficacy in the ischemic brain, providing several benefits. A major obstacle for the clinical translation of these therapies has been the inability to noninvasively monitor the best route, cell doses, and collateral effects, while ensuring survival and effective biological functioning of the transplanted stem cells. Combined image modalities have improved the accuracy of cellular therapy, allowed the *in vivo* monitoring of the biodistribution and viability of transplanted stem cells due to associated new tracers such as multimodal nanoparticles with new labels and covers, resulting in low toxicity

and longtime residence in cells.

Research motivation

Although meta-analyses have examined the benefits of cell transplantation in experimental stroke, low viable cell retention after transplantation in ischemic brain areas still represents the major obstacle to the successful clinical translation of cell-based stroke repair approaches. The multimodal imaging techniques provide morpho-functional information for studying pathological events following ischemia, associated with new tracers. These innovations will contribute to further our comprehension of stem cell transplantation, allowing the assessment of therapeutic effects on a molecular scale.

Research objectives

In this study, we aim to evaluate the sensitivity of triple-modal imaging of stem cells labeled with multimodal nanoparticles with different iron concentrations and their cellular viability *in vitro* as well as the correlation of the quantification of the iron load between different techniques (ICP-MS, MRI and NIRF. In addition, we seek to verify whether these images of stem cells labeled with multimodal nanoparticles maintain the same properties after application in a stroke model. The results will help us to better understand the biodistribution, sensitivity and viability of stem cells labeled with nanoparticles in sham and stroke models.

Research methods

Isolated and immunophenotypically characterized hBM-MSCs were transduced with a lentivirus for BLI evaluation *in vitro* and *in vivo*. In addition, MNP-IR750 that had previously been characterized (hydrodynamic size, zeta potential, and optical properties) were used for labeling these cells and analyzing cell viability *via* MTT and BLI assays. The internalization process and quantification of the iron load in different concentrations of MNP-IR750 were analyzed *via* MRI, NIRF, and ICP-MS. In the *in vivo* study, the same labeled cells were implanted in the sham group and stroke group at different times and MNP-IR750 concentrations (after 4 h and after 6 d of cell implantation) to evaluate the sensitivity of triple-modal images.

Research results

The collection and isolation of hBM-MSCs after immunophenotypic characterization was demonstrated to be adequate for human bone marrow samples. After the transduction of these cells with luciferase, we detected a maximum BLI intensity of 2.0×10^8 photons/s in 10^6 hBM-MSC samples. Evaluation of the physicochemical characteristics of MNP-IR750 showed an average hydrodynamic diameter of 38.2 ± 0.5 nm, a zeta potential of +29.2 ± 1.9 mV and adequate colloidal stability, without agglomeration over 18 h. The iron load internalization process in hBM-MSCs showed a strong relationship of the signal with the corresponding MNP labeling concentration based on MRI, ICP-MS and NIRF. Cellular viability in the highest MNP-IR750 concentration showed a reduction of less than 10% compared to the control. The correlation analysis of the MNP-IR750 load internalized by hBM-MSCs between the MRI, ICP-MS and NIRF techniques showed the same correlation coefficient of 0.99. The evaluation of BLI, NIRF, and MRI signals *in vivo* and *ex vivo* after labeled hBM-MSCs were implanted in the animals showed sensitivity in the detection of MNP-IR750 concentrations of 5, 20 and 50 μg Fe/mL at 4 h and 6 d in the sham groups, with significant results regarding the time and image effect as well as the group effect when the sham and stroke groups were compared at 6 d.

Research conclusions

Our study demonstrates that MNP-IR750 can be used to monitor cell grafts noninvasively, longitudinally, and repetitively, enabling the assessment of cell graft conditions *in vivo* after stroke for multimodal imaging assessment. The BLI signal of hBM-MSC_{Luc} showed the best imaging technique for functional and longitudinal assessment.

Research perspectives

In summary, we highlight the importance of quantification of multimodal nanoparticles internalized by cells and the efficacy of signal detection under the triple-image modality in a stroke model. However, the applicability of multimodal imaging should always be analyzed in accordance with the limitations and advantages of each technique involved.

REFERENCES

1 **Phinney DG**, Prockop DJ. Concise review: mesenchymal stem/multipotent stromal cells: the state of transdifferentiation and modes of tissue repair--current views. *Stem Cells* 2007; **25**: 2896-2902 [PMID: 17901396 DOI: 10.1634/stemcells.2007-0637]

2 **Alvarim LT**, Nucci LP, Mamani JB, Marti LC, Aguiar MF, Silva HR, Silva GS, Nucci-da-Silva MP, DelBel EA, Gamarra LF. Therapeutics with SPION-labeled stem cells for the main diseases related to brain aging: a systematic review. *Int J Nanomedicine* 2014; **9**: 3749-3770 [PMID: 25143726 DOI: 10.2147/IJN.S65616]

3 **Wu Y**, Zhao RC. The role of chemokines in mesenchymal stem cell homing to myocardium. *Stem Cell Rev* 2012; **8**: 243-250 [PMID: 21706142 DOI: 10.1007/s12015-011-9293-z]

4 **Eggenhofer E**, Luk F, Dahlke MH, Hoogduijn MJ. The life and fate of mesenchymal stem cells. *Front Immunol* 2014; **5**: 148 [PMID: 24904568 DOI: 10.3389/fimmu.2014.00148]

5 **Fischer UM**, Harting MT, Jimenez F, Monzon-Posadas WO, Xue H, Savitz SI, Laine GA, Cox CS.

Pulmonary passage is a major obstacle for intravenous stem cell delivery: the pulmonary first-pass effect. *Stem Cells Dev* 2009; **18**: 683-692 [PMID: 19099374 DOI: 10.1089/scd.2008.0253]
6 **Au P**, Hursh DA, Lim A, Moos MC, Oh SS, Schneider BS, Witten CM. FDA oversight of cell therapy clinical trials. *Sci Transl Med* 2012; **4**: 149fs31 [PMID: 22932219 DOI: 10.1126/scitranslmed.3004131]
7 **Kircher MF**, Gambhir SS, Grimm J. Noninvasive cell-tracking methods. *Nat Rev Clin Oncol* 2011; **8**: 677-688 [PMID: 21946842 DOI: 10.1038/nrclinonc.2011.141]
8 **Li X**, Zhang XN, Li XD, Chang J. Multimodality imaging in nanomedicine and nanotheranostics. *Cancer Biol Med* 2016; **13**: 339-348 [PMID: 27807501 DOI: 10.20892/j.issn.2095-3941.2016.0055]
9 **Lee DE**, Koo H, Sun IC, Ryu JH, Kim K, Kwon IC. Multifunctional nanoparticles for multimodal imaging and theragnosis. *Chem Soc Rev* 2012; **41**: 2656-2672 [PMID: 22189429 DOI: 10.1039/c2cs15261d]
10 **Yang HM**, Park CW, Park S, Kim JD. Cross-linked magnetic nanoparticles with a biocompatible amide bond for cancer-targeted dual optical/magnetic resonance imaging. *Colloids Surf B Biointerfaces* 2018; **161**: 183-191 [PMID: 29080502 DOI: 10.1016/j.colsurfb.2017.10.049]
11 **Gupta AK**, Gupta M. Synthesis and surface engineering of iron oxide nanoparticles for biomedical applications. *Biomaterials* 2005; **26**: 3995-4021 [PMID: 15626447 DOI: 10.1016/j.biomaterials.2004.10.012]
12 **Li J**, Lee WY, Wu T, Xu J, Zhang K, Hong Wong DS, Li R, Li G, Bian L. Near-infrared light-triggered release of small molecules for controlled differentiation and long-term tracking of stem cells in vivo using upconversion nanoparticles. *Biomaterials* 2016; **110**: 1-10 [PMID: 27693946 DOI: 10.1016/j.biomaterials.2016.09.011]
13 **Zhang W**, Wang W, Yu DX, Xiao Z, He Z. Application of nanodiagnostics and nanotherapy to CNS diseases. *Nanomedicine (Lond)* 2018; **13**: 2341-2371 [PMID: 30088440 DOI: 10.2217/nnm-2018-0163]
14 **Chen G**, Lin S, Huang D, Zhang Y, Li C, Wang M, Wang Q. Revealing the Fate of Transplanted Stem Cells In Vivo with a Novel Optical Imaging Strategy. *Small* 2018; **14** [PMID: 29171718 DOI: 10.1002/smll.201702679]
15 **Sarkar D**, Spencer JA, Phillips JA, Zhao W, Schafer S, Spelke DP, Mortensen LJ, Ruiz JP, Vemula PK, Sridharan R, Kumar S, Karnik R, Lin CP, Karp JM. Engineered cell homing. *Blood* 2011; **118**: e184-e191 [PMID: 22034631 DOI: 10.1182/blood-2010-10-311464]
16 **Sibov TT**, Pavon LF, Miyaki LA, Mamani JB, Nucci LP, Alvarim LT, Silveira PH, Marti LC, Gamarra L. Umbilical cord mesenchymal stem cells labeled with multimodal iron oxide nanoparticles with fluorescent and magnetic properties: application for in vivo cell tracking. *Int J Nanomedicine* 2014; **9**: 337-350 [PMID: 24531365 DOI: 10.2147/IJN.S53299]
17 **Souza TKF**, Nucci MP, Mamani JB, da Silva HR, Fantacini DMC, de Souza LEB, Picanço-Castro V, Covas DT, Vidoto EL, Tannús A, Gamarra LF. Image and motor behavior for monitoring tumor growth in C6 glioma model. *PLoS One* 2018; **13**: e0201453 [PMID: 30048545 DOI: 10.1371/journal.pone.0201453]
18 **Mamani JB**, Pavon LF, Miyaki LA, Sibov TT, Rossan F, Silveira PH, Cárdenas WH, Amaro Junior E, Gamarra LF. Intracellular labeling and quantification process by magnetic resonance imaging using iron oxide magnetic nanoparticles in rat C6 glioma cell line. *Einstein (Sao Paulo)* 2012; **10**: 216-221 [PMID: 23052458 DOI: 10.1590/S1679-45082012000200016]
19 **Gamarra LF**, Amaro E, Alves S, Soga D, Pontuschka WM, Mamani JB, Carneiro SM, Brito GE, Figueiredo Neto AM. Characterization of the biocompatible magnetic colloid on the basis of Fe3O4 nanoparticles coated with dextran, used as contrast agent in magnetic resonance imaging. *J Nanosci Nanotechnol* 2010; **10**: 4145-4153 [PMID: 21128393 DOI: 10.1166/jnn.2010.2200]
20 **Paxinos G**, Watson Ch. The Rat Brain in Stereotaxic Coordinates. London: Academic Press 1998;
21 **da Silva H**, Nucci MP, Mamani JB, Mendez-Otero R, Nucci LP, Tannus A, Gamarra LF. Evaluation of temperature induction in focal ischemic thermocoagulation model. *PLoS One* 2018; **13**: e0200135 [PMID: 29975761 DOI: 10.1371/journal.pone.0200135]
22 **Giraldi-Guimardes A**, Rezende-Lima M, Bruno FP, Mendez-Otero R. Treatment with bone marrow mononuclear cells induces functional recovery and decreases neurodegeneration after sensorimotor cortical ischemia in rats. *Brain Res* 2009; **1266**: 108-120 [PMID: 19368806 DOI: 10.1016/j.brainres.2009.01.062]
23 **Nucci LP**, Silva HR, Giampaoli V, Mamani JB, Nucci MP, Gamarra LF. Stem cells labeled with superparamagnetic iron oxide nanoparticles in a preclinical model of cerebral ischemia: a systematic review with meta-analysis. *Stem Cell Res Ther* 2015; **6**: 27 [PMID: 25889904 DOI: 10.1186/s13287-015-0015-3]
24 **Saadatpour Z**, Rezaei A, Ebrahimnejad H, Baghaei B, Bjorklund G, Chartrand M, Sahebkar A, Morovati H, Mirzaei HR, Mirzaei H. Imaging techniques: new avenues in cancer gene and cell therapy. *Cancer Gene Ther* 2017; **24**: 1-5 [PMID: 27834357 DOI: 10.1038/cgt.2016.61]
25 **Key J**, Leary JF. Nanoparticles for multimodal in vivo imaging in nanomedicine. *Int J Nanomedicine* 2014; **9**: 711-726 [PMID: 24511229 DOI: 10.2147/IJN.S53717]
26 **Dabrowska S**, Del Fattore A, Karnas E, Frontczak-Baniewicz M, Kozlowska H, Muraca M, Janowski M, Lukomska B. Imaging of extracellular vesicles derived from human bone marrow mesenchymal stem cells using fluorescent and magnetic labels. *Int J Nanomedicine* 2018; **13**: 1653-1664 [PMID: 29593411 DOI: 10.2147/IJN.S159404]
27 **Ma L**, Li MW, Bai Y, Guo HH, Wang SC, Yu Q. Biological Characteristics of Fluorescent Superparamagnetic Iron Oxide Labeled Human Dental Pulp Stem Cells. *Stem Cells Int* 2017; **2017**: 4837503 [PMID: 28298928 DOI: 10.1155/2017/4837503]
28 **Zhang X**, Bloch S, Akers W, Achilefu S. Near-infrared molecular probes for in vivo imaging. *Curr Protoc Cytom* 2012; **Chapter** 12: Unit12.27 [PMID: 22470154 DOI: 10.1002/0471142956.cy1227s60]
29 **Lee N**, Choi Y, Lee Y, Park M, Moon WK, Choi SH, Hyeon T. Water-dispersible ferrimagnetic iron oxide nanocubes with extremely high r relaxivity for highly sensitive in vivo MRI of tumors. *Nano Lett* 2012; **12**: 3127-3131 [PMID: 22575047 DOI: 10.1021/nl3010308]
30 **Korchinski DJ**, Taha M, Yang R, Nathoo N, Dunn JF. Iron Oxide as an MRI Contrast Agent for Cell Tracking. *Magn Reson Insights* 2015; **8**: 15-29 [PMID: 26483609 DOI: 10.4137/MRI.S23557]
31 **Chopp M**, Li Y. Treatment of neural injury with marrow stromal cells. *Lancet Neurol* 2002; **1**: 92-100 [PMID: 12849513 DOI: 10.1016/S1474-4422(02)00040-6]
32 **Kim HJ**, Park JS. Usage of Human Mesenchymal Stem Cells in Cell-based Therapy: Advantages and Disadvantages. *Dev Reprod* 2017; **21**: 1-10 [PMID: 28484739 DOI: 10.12717/DR.2017.21.1.001]
33 **Yousefifard M**, Nasirinezhad F, Shardi Manaheji H, Janzadeh A, Hosseini M, Keshavarz M. Human bone marrow-derived and umbilical cord-derived mesenchymal stem cells for alleviating neuropathic pain in a spinal cord injury model. *Stem Cell Res Ther* 2016; **7**: 36 [PMID: 26957122 DOI: 10.1186/s13287-016-0295-2]

34 **Li XY**, Ding J, Zheng ZH, Li XY, Wu ZB, Zhu P. Long-term culture in vitro impairs the immunosuppressive activity of mesenchymal stem cells on T cells. *Mol Med Rep* 2012; **6**: 1183-1189 [PMID: 22923041 DOI: 10.3892/mmr.2012.1039]

35 **Moore TL**, Rodriguez-Lorenzo L, Hirsch V, Balog S, Urban D, Jud C, Rothen-Rutishauser B, Lattuada M, Petri-Fink A. Nanoparticle colloidal stability in cell culture media and impact on cellular interactions. *Chem Soc Rev* 2015; **44**: 6287-6305 [PMID: 26056687 DOI: 10.1039/c4cs00487f]

36 **Myers D**. Surfaces, interfaces, and colloids: principles and applications. New York: Wiley-VCH Publishers 1999; 40-78

37 **Zhang Y**, Yang M, Portney NG, Cui D, Budak G, Ozbay E, Ozkan M, Ozkan CS. Zeta potential: a surface electrical characteristic to probe the interaction of nanoparticles with normal and cancer human breast epithelial cells. *Biomed Microdevices* 2008; **10**: 321-328 [PMID: 18165903 DOI: 10.1007/s10544-007-9139-2]

38 **Hu L**, Mao Z, Gao Ch. Colloidal particles for cellular uptake and delivery. *J Mater Chem* 2009; **19**: 3108-3115 [DOI: 10.1039/B815958K]

39 **Cai YR**, Liu YK, Yan WQ, Hu QH, Tao JH, Zhang M, Shi ZL, Tang RK. Role of hydroxyapatite nanoparticle size in bone cell proliferation. *J Mater Chem* 2007; **17**: 3780-3787 [DOI: 10.1039/B705129H]

40 **Montet-Abou K**, Montet X, Weissleder R, Josephson L. Cell internalization of magnetic nanoparticles using transfection agents. *Mol Imaging* 2007; **6**: 1-9 [PMID: 17311760 DOI: 10.2310/7290.2006.00028]

41 **Lee JH**, Jung MJ, Hwang YH, Lee YJ, Lee S, Lee DY, Shin H. Heparin-coated superparamagnetic iron oxide for in vivo MR imaging of human MSCs. *Biomaterials* 2012; **33**: 4861-4871 [PMID: 22475532 DOI: 10.1016/j.biomaterials.2012.03.035]

42 **Vaněček V**, Zablotskii V, Forostyak S, Růžička J, Herynek V, Babič M, Jendelová P, Kubinová S, Dejneka A, Syková E. Highly efficient magnetic targeting of mesenchymal stem cells in spinal cord injury. *Int J Nanomedicine* 2012; **7**: 3719-3730 [PMID: 22888231 DOI: 10.2147/IJN.S32824]

43 **Adams CF**, Pickard MR, Chari DM. Magnetic nanoparticle mediated transfection of neural stem cell suspension cultures is enhanced by applied oscillating magnetic fields. *Nanomedicine* 2013; **9**: 737-741 [PMID: 23751375 DOI: 10.1016/j.nano.2013.05.014]

44 **Addicott B**, Willman M, Rodriguez J, Padgett K, Han D, Berman D, Hare JM, Kenyon NS. Mesenchymal stem cell labeling and in vitro MR characterization at 1.5 T of new SPIO contrast agent: Molday ION Rhodamine-B™. *Contrast Media Mol Imaging* 2011; **6**: 7-18 [PMID: 20690161 DOI: 10.1002/cmmi.396]

45 **Townsend D**, Cheng Zh, Georg D, Drexler W, Moser E; Townsend D, Cheng Zh, Georg D, Drexler W, Moser E. Grand challenges in biomedical physics. *Front Phys* 2013; **1**: 1-6 [DOI: 10.3389/fphy.2013.00001]

46 **Duan X**, Lu L, Wang Y, Zhang F, Mao J, Cao M, Lin B, Zhang X, Shuai X, Shen J. The long-term fate of mesenchymal stem cells labeled with magnetic resonance imaging-visible polymersomes in cerebral ischemia. *Int J Nanomedicine* 2017; **12**: 6705-6719 [PMID: 28932115 DOI: 10.2147/IJN.S146742]

47 **Schweiger C**, Hartmann R, Zhang F, Parak WJ, Kissel TH, Rivera Gil P. Quantification of the internalization patterns of superparamagnetic iron oxide nanoparticles with opposite charge. *J Nanobiotechnology* 2012; **10**: 28 [PMID: 22781560 DOI: 10.1186/1477-3155-10-28]

48 **Vandeputte C**, Thomas D, Dresselaers T, Crabbe A, Verfaillie C, Baekelandt V, Van Laere K, Himmelreich U. Characterization of the inflammatory response in a photothrombotic stroke model by MRI: implications for stem cell transplantation. *Mol Imaging Biol* 2011; **13**: 663-671 [PMID: 20700767 DOI: 10.1007/s11307-010-0395-9]

49 **Dadashzadeh ER**, Hobson M, Henry Bryant L, Dean DD, Frank JA. Rapid spectrophotometric technique for quantifying iron in cells labeled with superparamagnetic iron oxide nanoparticles: potential translation to the clinic. *Contrast Media Mol Imaging* 2013; **8**: 50-56 [PMID: 23109392 DOI: 10.1002/cmmi.1493]

50 **Aswendt M**, Adamczak J, Tennstaedt A. A review of novel optical imaging strategies of the stroke pathology and stem cell therapy in stroke. *Front Cell Neurosci* 2014; **8**: 226 [PMID: 25177269 DOI: 10.3389/fncel.2014.00226]

51 **Jang KS**, Lee KS, Yang SH, Jeun SS. In vivo Tracking of Transplanted Bone Marrow-Derived Mesenchymal Stem Cells in a Murine Model of Stroke by Bioluminescence Imaging. *J Korean Neurosurg Soc* 2010; **48**: 391-398 [PMID: 21286474 DOI: 10.3340/jkns.2010.48.5.391]

52 **Karp JM**, Leng Teo GS. Mesenchymal stem cell homing: the devil is in the details. *Cell Stem Cell* 2009; **4**: 206-216 [PMID: 19265660 DOI: 10.1016/j.stem.2009.02.001]

53 **Gurtner GC**, Werner S, Barrandon Y, Longaker MT. Wound repair and regeneration. *Nature* 2008; **453**: 314-321 [PMID: 18480812 DOI: 10.1038/nature07039]

54 **Santoso MR**, Yang PC. Magnetic Nanoparticles for Targeting and Imaging of Stem Cells in Myocardial Infarction. *Stem Cells Int* 2016; **2016**: 4198790 [PMID: 27127519 DOI: 10.1155/2016/4198790]

55 **Zhang F**, Duan X, Lu L, Zhang X, Chen M, Mao J, Cao M, Shen J. In Vivo Long-Term Tracking of Neural Stem Cells Transplanted into an Acute Ischemic Stroke model with Reporter Gene-Based Bimodal MR and Optical Imaging. *Cell Transplant* 2017; **26**: 1648-1662 [PMID: 29251112 DOI: 10.1177/0963689717722560]

56 **Dimmeler S**, Ding S, Rando TA, Trounson A. Translational strategies and challenges in regenerative medicine. *Nat Med* 2014; **20**: 814-821 [PMID: 25100527 DOI: 10.1038/nm.3627]

P- Reviewer: Grawish ME, Hassan AI, Haider KH

S- Editor: Ma YJ **L- Editor:** A **E- Editor:** Bian YN

Baishideng®

Published By Baishideng Publishing Group Inc
7901 Stoneridge Drive, Suite 501, Pleasanton, CA 94588, USA
Telephone: +1-925-2238242
Fax: +1-925-2238243
E-mail: bpgoffice@wjgnet.com
Help Desk: https://www.f6publishing.com/helpdesk
https://www.wjgnet.com